Department of Electronic and Computer Engineering
Technical University of Crete

THESIS

Modeling Video Traffic from Multiplexed H.264 Video Streams

VASILEIADOU DIMITRA

CHANIA

August, 2011

Supervisor: Prof. Polychronis Koutsakis

ACKNOWLEDGMENTS

I wish to thank all those who helped me complete my thesis.

Firstly, I am heartily thankful to my supervisor, Polychronis Koutsakis, for giving me the opportunity to work with him and for his encouragement, guidance and support from the initial to the final level, which enabled me to develop an understanding of the subject.

I would like to thank Professors Michael Paterakis and Michael Zervakis for their participation in the examination committee.

In addition, many thanks to Charalampos Stamos, Michael Argyriou, Aggelos Lazaris and Konstantinos Achladianakis for their important contribution to the completion of this thesis.

Finally, I would like to give my special thanks to my family and my friends for their love and support in every way possible.

Abstract

As traffic from video services is expected to be a substantial portion of the traffic carried by emerging wired and wireless networks, statistical source models are needed for Variable Bit Rate (VBR) coded video in order to design networks which are able to guarantee the strict Quality of Service (QoS) requirements of the video traffic. Video packet delay requirements are strict, because delays are annoying to a viewer; when the delay experienced by a video packet exceeds the corresponding maximum delay, the packet is dropped and the video packet dropping requirements are equally strict. Hence, the problem of modeling video traffic becomes especially significant.

H.264 is the latest video coding standard of the ITU-T Video Coding Experts Group (VCEG) and the ISO/IEC Moving Picture Experts Group (MPEG). It has recently become the most widely accepted video coding standard since the deployment of MPEG2 at the dawn of digital television. It covers all common video applications ranging from mobile services and videoconferencing to IPTV, HDTV, and HD video storage.

Previous work on modeling video traffic (mainly videoconference) coded with past encoding standards found that the marginal distributions for all the sequences could be described by a gamma or Pearson V distribution and used this result to build a Discrete Autoregressive (DAR) model of order one, which works well when several sources are multiplexed. Our study focuses on the problem of modeling video (i.e., not videoconference) traffic from H.264 encoders, which is a relatively new and yet open issue in the relevant literature. Our results reveal significant differences with the results of the past relevant literature, but still show that the DAR(1) model can provide a reliable modeling approach for more than half of the cases studied.

TABLE OF CONTENTS

1. INTRODUCTION…………………………………………………………………5

2. SINGLE-SOURCE H.264 TRAFFIC MODELING………………………………8

    2.1 Distributions…………………………………………………………………..9

    2.2 Statistical Tests……………………………………………………………….10

    2.3 Statistical Tests' Results……………………………………………………...12

    2.4 Finding the best fits…………………………………………………………..23

3. MODELING MULTIPLEXED H.264 VIDEO TRAFFIC………………………..26

    3.1 The DAR(1) Model…………………………………………………………..26

    3.2 Modeling results and discussion based on Q-Q plots test……………………31

4. CONCLUSIONS………………………………………………………………..32

REFERENCES…………………………………………………………………….34

APPENDIX A……………………………………………………………………..37

APPENDIX B……………………………………………………………………..46

1. INTRODUCTION

As traffic from video services is expected to be a substantial portion of the traffic carried by emerging wired and wireless networks [1][2], statistical source models are needed for Variable Bit Rate (VBR) coded video in order to design networks which are able to guarantee the strict Quality of Service (QoS) requirements of the video traffic. Video packet delay requirements are strict, because delays are annoying to a viewer; when the delay experienced by a video packet exceeds the corresponding maximum delay, the packet is dropped and the video packet dropping requirements are equally strict.

Hence, the problem of modeling video traffic has been extensively studied in the literature. VBR video models which have been proposed in the literature include first-order autoregressive (AR) models [4], discrete AR (DAR) models [3][5], Markov renewal processes (MPR) [6], MPR transform-expand-sample (TES) [7], finite state Markov chain [8], Gamma-beta-auto-regression (GBAR) models [9][10], discrete-time Semi-Markov Processes (SMP) [11], wavelets [12] multifractal and fractal methods [13].

H.264 is the latest video coding standard of the ITU-T Video Coding Experts Group (VCEG) and the ISO/IEC Moving Picture Experts Group (MPEG). It has recently become the most widely accepted video coding standard since the deployment of MPEG2 at the dawn of digital television, and it may soon overtake MPEG2 in common use [16]. It covers all common video applications ranging from mobile services and videoconferecing to IPTV, HDTV, and HD video storage.

Standard H.264 encoders generate three types of video frames: I (intra-coded), P (predictive) and B (bidirectionally predictive); i.e., while I frames are intra-coded, the generation of P and B frames involves, in addition to intra-coding, the use of motion prediction and interpolation techniques. I frames are, on average, the largest in size, followed by P and then by B frames.

The video coding layer of H.264/AVC (Advanced Video Codec) is similar to that of other video coding standards such as MPEG2 Video. In fact, it uses a fairly traditional approach consisting of a hybrid of block-based temporal and spatial prediction in conjunction with block-based transform coding [16]. In 2007, the Scalable Video Coding (SVC) extension has been added to the H.264/AVC standard. The SVC extension provides temporal scalability, Coarse Grain Scalability (CGS), Medium Grain Scalability (MGS), and SNR scalability in general, spatial scalability, and combined spatiotemporal-SNR scalability [17]. The study of H.264/SVC is out of the scope of this thesis. In the rest of the thesis, we use the term “H.264” to refer to the H.264/AVC video standard

Similarly to the work in [18][24] on modeling videoconference traffic, our work focuses on the accurate fitting of the marginal (stationary) distribution of video frame sizes of single H.264 video traces. More specifically, our work follows the steps of the work presented in [5], where Heyman et al. analyzed three videoconference sequences coded with a modified version of the H.261 video coding standard and two other coding schemes, similar to the H.261. The authors in [5] found that the marginal distributions for all the sequences could be described by a gamma (or equivalently, negative binomial) distribution and used this result to build a Discrete Autoregressive (DAR) model of order one, which works well when several sources are multiplexed. In [18], the authors found that the marginal distributions for all H.263 videoconference sequences could be described by a Pearson V distribution. The same result was the product of the study in [24] which focused on H.264 videoconference traffic.

An important feature of common H.264 encoders is the manner in which frame types are generated. Typical encoders use a fixed Group-Of-Pictures (GOP) pattern when compressing a video sequence; the GOP pattern specifies the number and temporal order of P and B frames between two successive I frames. A GOP pattern is defined by the distance N between I frames and the distance M between P frames.

In this work, we focus on the problem of modeling video (i.e., not videoconference) traffic from H.264 encoders, which is a relatively new and yet open issue in the relevant literature.

2. SINGLE-SOURCE H.264 TRAFFIC MODELING

The first step in our modeling approach is to analyze the statistical behavior of single-source H.264 video traces. We perform a statistical testing analysis by using three well-known statistical tests, which will be presented later in Section 2.

In our work, we have studied 9 different long sequences of H.264 VBR encoded videos in 196 formats, from the publicity available Video Trace Library of [19], in order to derive a statistical model which fits well the real data.

The traces used are in Common Intermediate Format (CIF)(i.e. 352x288 pixels) and in High Definition (HD) 720 and 1080 format (i.e. 1280x720p and 1920x1080i, respectively). We have used, from [19], all the different Quantization Parameters (QP) for each of the traces under study. The 9 traces are: Tokyo Olympics, Silence of the Lambs, Star Wars IV, Sony Demo, NBC News, Terminator 2, KAET's From Mars to China, KAET's Horizon (Jan.6, 2006) and Sony Demo. The length of the videos is 74, 30 and 10 minutes, as shown in Table 1. Appendix A includes the data on the mean, peak and standard deviation of each trace under study.

TABLE 1. TRACE FORMAT AND VIDEO LENGTH

	Trace	Format	Video's length
1	Tokyo Olympics	CIF	74 min
2	Silence of the Lambs	CIF	30 min
3	Star Wars IV	CIF	30 min
4	Sony Demo	CIF	10 min
5	NBC News	CIF	30 min
6	Terminator 2	HD	10 min
7	KAET's From Mars to China	HD	30 min
8	KAET's Horizon (Jan.6, 2006)	HD	30 min
9	Sony Demo	HD	10 min

The data for each trace consists of a sequence of the number of cells per video frame and the type of video frame, i.e. I, P or B. Without loss of generality, we use

48-byte packets throughout this work, but our modeling approach can be used equally well with packets of other sizes.

We have investigated the possibility of modeling the 196 traces with quite a few well-known distributions (exponential, gamma, lognormal, weibull, pearson V, geometric and negative binomial) [20]. Since almost all (with the exception of the exponential) of the above-mentioned distributions have been often used for video traffic modeling in the literature, they have been included in this work as fitting candidates, in order to compare their results in the case of H.264 video modeling.

2.1. Distributions

In this section we present the Probability Density Function (PDF), the mean and the variance of the distributions that we used in our study.

- The PDF of an exponential distribution with parameter b>0 is $f(x) = \frac{1}{b} e^{-x/b}$ for all x≥0 and zero otherwise. The mean and variance are given by the following equations: $Mean = b$, $Variance = b^2$.
- The PDF of a gamma distribution with parameters (a, b) , a>0 and b>0, is $f(x) = \frac{b^{-a} x^{a-1} e^{-x/b}}{\Gamma(a)}$ for all x≥0 and zero otherwise. The mean and variance are given by the following equations: $Mean = ab$, $Variance = ab^2$.
- The PDF of a lognormal distribution with parameters (μ, σ^2), μ>0 and σ>0, is $f(x) = \frac{1}{x\sqrt{2\pi\sigma^2}} \exp\left(\frac{-(lnx-\mu)^2}{2\sigma^2}\right)$, for all x≥0 and zero otherwise. The mean and variance are given by the following equations: $Mean = e^{\mu+\frac{\sigma^2}{2}}$, $Variance = e^{2\mu+\sigma^2}(e^{\sigma^2} - 1)$.

- The PDF of a weibull distribution with parameters (a, b) , a>0 and b>0, is $f(x) = ab^{-a}x^{a-1}e^{-(x/b)^a}$, for all x≥0 and zero otherwise. The mean and variance are given by the following equations: $Mean = \frac{b}{a}\Gamma\left(\frac{1}{a}\right)$, $Variance = \frac{b^2}{a}\left\{2\Gamma\left(\frac{2}{a}\right) - \frac{1}{a}\left[\Gamma\left(\frac{1}{a}\right)\right]^2\right\}$.

- The PDF of a pearson V distribution with parameters (a, b), a>0 and b>0, is $(x) = \frac{x^{-(a+1)}e^{-b/x}}{b^{-a}\Gamma(a)}$, for all x≥0 and zero otherwise. The mean and variance are given by the following equations: $Mean = \frac{b}{a-1}$ for a>1, $Variance = \frac{b^2}{(a-1)^2(a-2)}$ for a>2.

- The PDF of a geometric distribution with parameter p in (0, 1) is $p(x) = p(1-p)^x$, for all x in {0,1, . . .} and zero otherwise. The mean and variance are given by the following equations: $Mean = \frac{1-p}{p}$, $Variance = \frac{1-p}{p^2}$.

- The PDF of a negative binomial distribution with parameters (s, p), s is a positive integer and p is in (0, 1), is $p(x) = \binom{s+x-1}{x}p^s(1-p)^x$, for all x in {0, 1} and zero otherwise. The mean and variance are given by the following equations: $Mean = \frac{s(1-p)}{p}$, $Variance = \frac{s(1-p)}{p^2}$.

2.2. Statistical Tests

In this section we report the statistical tests used in our study. They include qualitative tests like Q-Q plots [5][20], and quantitative tests like Kolmogorov-Smirnov tests [20] and Kullback-Leiber divergence tests [21].

2.2.1. Q-Q plots test

The Q-Q plot is a powerful goodness-of-fit test, which graphically compares two data sets in order to determine whether the data sets come from populations with a common distribution (if they do, the points of the plot should fall approximately along a 45-degree reference line). More specifically, a Q-Q plot is a plot of the quantiles of the real data versus the quantiles of the fitted distribution (statistic data). A z-quantile of X is any value x such that: $P((X \leq x) = z)$

2.2.2. Kolmogorov-Smornov test

The Kolmogorov-Smornov test (KS-test) tries to determine if two datasets differ significantly. The KS-test has the advantage of making no assumption about the distribution of data, i.e. it is non-parametric and distribution free. The KS-test uses the maximum vertical deviation between the two curves as its statistic D which is defined as follows: $D = \sup_x\{|F(x) - G(x)|\}$ where F(x) and G(x) are the empirical distribution function of the original data and the cumulative distribution function of the model, respectively.

2.2.3. The Kullback-Leiber divergence test

The Kullback-Leibler divergence test (KL-test) is a measure of the difference between two probability distributions *f* and *g* and is defined as follows:

$$I(f,g) = \sum_{i=1}^{k} p_i \log\left(\frac{p_i}{\pi_i}\right)$$

where *log* denotes the natural logarithm. Here, there are k possible outcomes of the underlying random variable; the true probability of the i^{th} outcome is given by p_i, while the $\pi_1, \ldots, \pi_k$ constitute the approximating probability distribution (i.e., the approximating model). In this case, we have $0 < p_i < 1$, $0 < \pi_i < 1$, and $\sum p_i = \sum \pi_i = 1$. Hence, here f and g correspond to the p_i and π_i, respectively. The notation $I(f, g)$ denotes the information lost when g is used to approximate f or the distance from g to f. If the quantity 0log0 appears in the formula, it is interpreted as zero.

2.3. Statistical Tests' Results

In this section we report our Q-Q plot tests' results when trying to find the best fit for all video frame sizes (i.e., we study the video trace as a whole, without discriminating between different video frames types). Our results are presented in Table 2.

TABLE 2. Q-Q PLOTS' RESULTS FOR BEST DISTRIBUTION FIT (TRACE AS A WHOLE)

distribution	results per distribution
exponential	0%
gamma	51%
lognormal	10%
weibull	36%
pearsonV	2%
geometric	1%
negative binomial	0%

Although these distributions were shown to be the better fit in comparison to the others, the fit was not perfectly accurate in none of the cases studied. This was expected, as the gross differences in the number of bits required to represent I, P and B frames impose a degree of periodicity on H.264-encoded streams, based on the cyclic GoP formats.

Hence, we proceeded to study the frame size distribution for each of the three different video frame types (I, P, B), in the same way we studied the frame size distribution for the whole trace. This approach was also used in [10][23].

The mean, peak and variance of the video frame sizes for each video frame type (I, P and B) of each movie were taken again from [19] and the distributions parameters calculated based on the formulae for the mean and variance presented in Section 2.1.

A few of our Q-Q plot tests' results are presented indicatively in Figures 1-8, where we present 2 examples of the results of Q-Q plots, KS and K-L statistical tests' results for the whole trace and for each type of frame separately. The fitting results when modeling each video frame type separately are clearly better than the results produced when modeling the trace as a whole. Our Q-Q plot tests' results, when studying I, P and B frames separately, are summarized in Tables 3 and 4. Table 3 presents the cumulative results per distribution, while Table 4 presents the fitting results for each type of video frame. Our respective results with the use of the KS test are summarized in Tables 5-6, and with the use of the K-L test are summarized in Tables 7-8.

Example 1: "KAET's From Mars to China G12B2

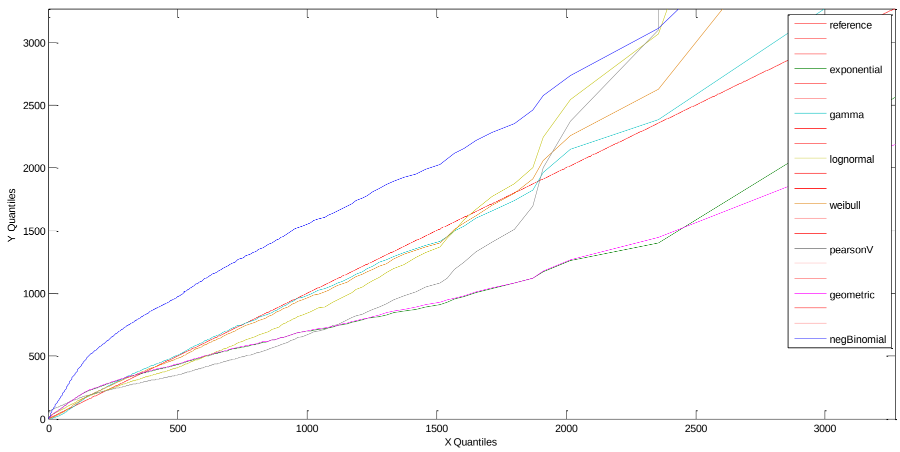

Figure 1.a. Q-Q plots for the whole KAET's From Mars to China trace. The best fit is provided by the gamma distribution.

```
kstest =

    0.1498          exponential
    0.1145          gamma
    0.1179          lognormal
    0.0507          weibull
    0.2970          pearsonV
    0.1490          geometric
    0.3764          negative Binomial


kltest =

    1.8917          exponential
    3.1457          gamma
    1.9018          lognormal
    2.6076          weibull
    1.4913          pearsonV
    1.8720          geometric
    1.8868          negative Binomial
```

Figure 1.b. KS and KL tests' results for the whole KAET's From Mars to China. The best fit is provided by the gamma distribution.

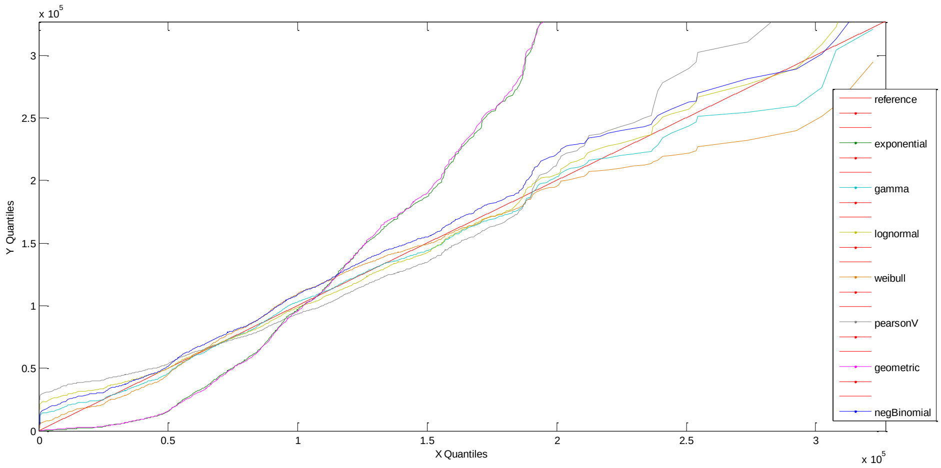

Figure 2.a. Q-Q plots for the I frames of KAET's From Mars to China trace. The best fit is provided by the gamma distribution.

```
kstest =

    0.2647    exponential
    0.0364    gamma
    0.0378    lognormal
    0.0694    weibull
    0.0654    pearsonV
    0.2719    geometric
    0.0645    negative Binomial


kltest =

    1.0287    exponential
    0.3887    gamma
    0.3675    lognormal
    0.4245    weibull
    0.3376    pearsonV
    1.0089    geometric
    0.3731    negative Binomial
```

Figure 2.b. KS and KL tests' results for the I frames of KAET's From Mars to China trace. The best fit is provided by the gamma distribution.

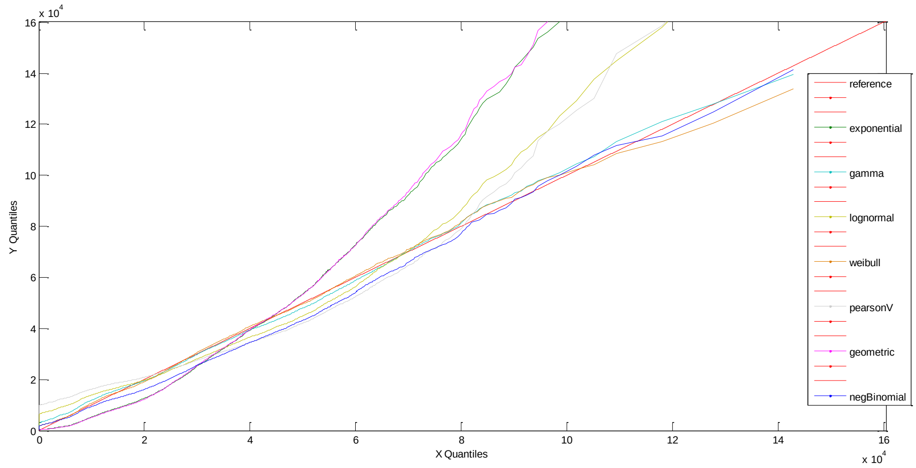

Figure 3.a. Q-Q plots for the P frames of KAET's From Mars to China trace. The best fit is provided by the weibull distribution.

```
kstest =

     0.1486     exponential
     0.0407     gamma
     0.0950     lognormal
     0.0218     weibull
     0.1576     pearsonV
     0.1468     geometric
     0.1090     negative Binomial


kltest =

     1.1317     exponential
     0.6525     gamma
     0.5855     lognormal
     0.7116     weibull
     0.5190     pearsonV
     1.1758     geometric
     0.7113     negative Binomial
```

Figure 3.b. KS and KL tests' results for the P frames of KAET's From Mars to China trace. The best fit is provided by the weibull distribution.

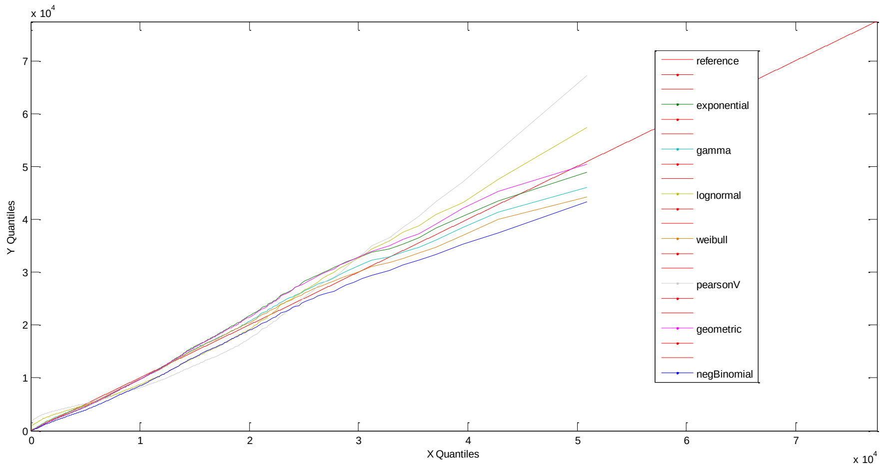

Figure 4.a. Q-Q plots for the B frames of KAET's From Mars to China trace. The best fit is provided by the gamma distribution.

```
kstest =

    0.0383        exponential
    0.0331        gamma
    0.1352        lognormal
    0.0236        weibull
    0.2267        pearsonV
    0.0339        geometric
    0.0863        negative Binomial


kltest =

    1.3718        exponential
    1.2781        gamma
    1.0047        lognormal
    1.2886        weibull
    0.8646        pearsonV
    1.3794        geometric
    1.3844        negative Binomial
```

Figure 4.b. KS and KL tests' results for the B frames of KAET's From Mars to China trace. The best fit is provided by the gamma distribution.

Example 2: NBC News G16B1 QP38

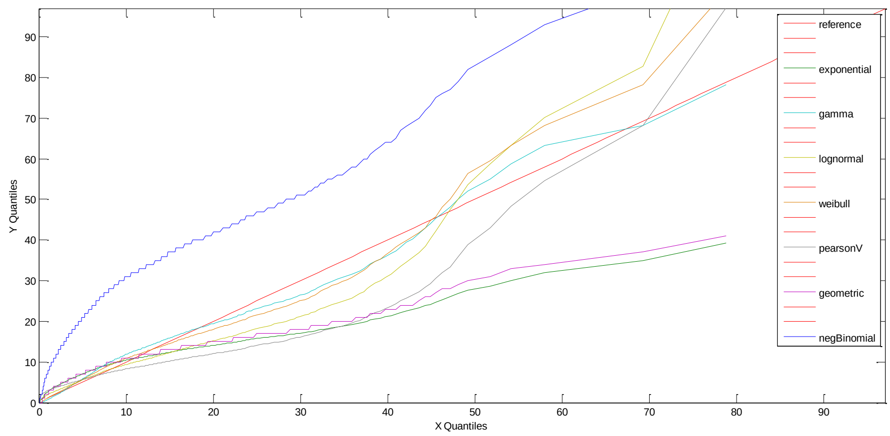

Figure 5.a. Q-Q plots for the whole NBC News(G16B1 QP38) trace. The best fit is provided by the gamma distribution.

```
kstest =

    0.2264    exponential
    0.2529    gamma
    0.1808    lognormal
    0.1492    weibull
    0.3983    pearsonV
    0.2276    geometric
    0.4736    negative Binomial


kltest =

    2.1606    exponential
    4.4031    gamma
    2.3211    lognormal
    3.3600    weibull
    1.7735    pearsonV
    2.1223    geometric
    2.1678    negative Binomial
```

Figure 5.b. KS and KL tests' results for the whole NBC News(G16B1 QP38) trace. The best fit is provided by the gamma distribution.

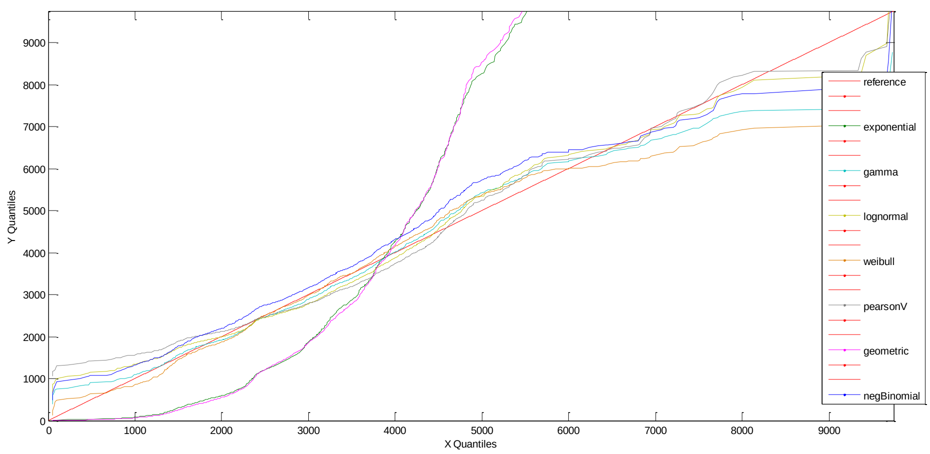

Figure 6.a. Q-Q plots for the I frames of NBC News(G16B1 QP38) trace. The best fit is provided by the pearson V distribution.

```
kstest =

    0.2907      exponential
    0.0436      gamma
    0.0740      lognormal
    0.0536      weibull
    0.0946      pearsonV
    0.3004      geometric
    0.0856      negative Binomial


kltest =

    0.9046      exponential
    0.2654      gamma
    0.2546      lognormal
    0.2845      weibull
    0.2277      pearsonV
    0.9742      geometric
    0.2579      negative Binomial
```

Figure 6.b KL and KS tests' results for the I frames of NBC News(G16B1 QP38) trace. The best fit is provided by the pearson V distribution.

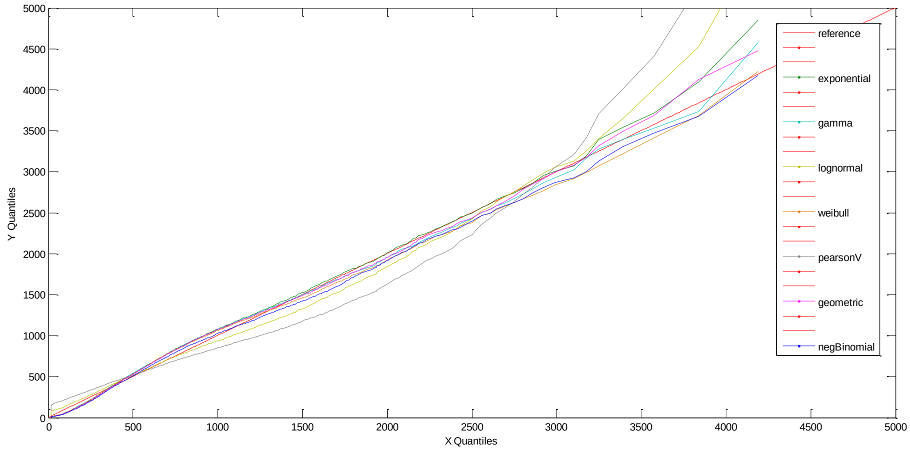

Figure 7.a. Q-Q plots for the P frames of NBC News(G16B1 QP38) trace. The best fit is provided by the gamma distribution.

```
kstest =

    0.0734    exponential
    0.0635    gamma
    0.0522    lognormal
    0.0662    weibull
    0.1640    pearsonV
    0.0721    geometric
    0.0809    negative Binomial


kltest =

    1.3838    exponential
    1.3407    gamma
    1.0167    lognormal
    1.3246    weibull
    0.8734    pearsonV
    1.3764    geometric
    1.3830    negative Binomial
```

Figure 7.b. KL and KS tests' results for the P frames of NBC News(G16B1 QP38) race. The best fit is provided by the gamma distribution.

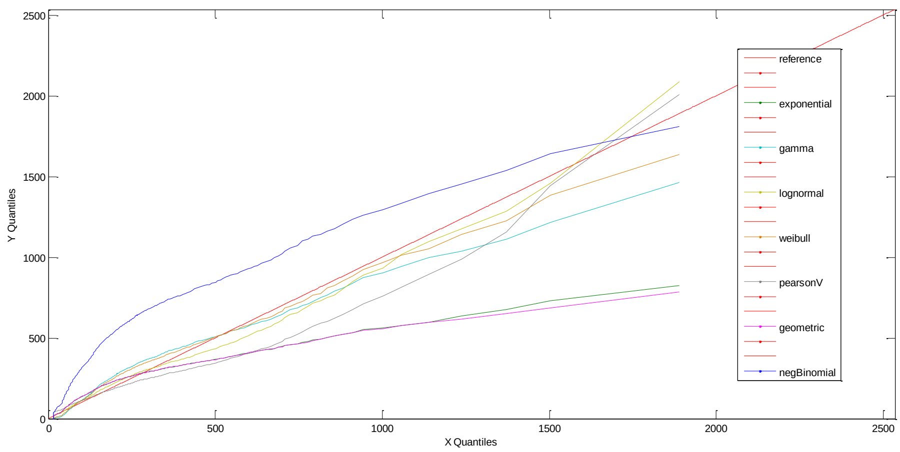

Figure 8. Q-Q plots for the B frames of NBC News(G16B1 QP38) trace. The best fit is provided by the lognormal distribution.

```
kstest =

      0.1290      exponential
      0.3337      gamma
      0.1063      lognormal
      0.2750      weibull
      0.2002      pearsonV
      0.1342      geometric
      0.3822      negative Binomial


kltest =

      1.7256      exponential
      3.0488      gamma
      1.7495      lognormal
      2.5236      weibull
      1.3211      pearsonV
      1.7634      geometric
      1.6921      negative Binomial
```

Figure 8.b. KL and KS tests' results for the B frames of NBC News(G16B1 QP38) trace. The best fit is provided by the lognormal distribution.

TABLE 3. Q-Q PLOTS' CUMULATIVE RESULTS FOR BEST DISTRIBUTION FIT (I, P, B FRAMES SEPARATELY)

distribution	results per distribution
exponential	1.5%
gamma	25%
lognormal	25.5%
weibull	36%
pearsonV	10%
geometric	0%
negative binomial	2%

TABLE 4. Q-Q PLOTS' RESULTS FOR BEST DISTRIBUTION FIT FOR EACH VIDEO FRAME TYPE

distribution	results per distribution I frames	results per distribution P frames	results per distribution B frames
exponential	0%	1%	2%
gamma	20.5%	37%	20%
lognormal	28%	20%	27%
weibull	28%	38%	42%
pearsonV	20.5%	3%	7%
geometric	0%	0.5%	1%
negative binomial	3%	0.5%	1%

TABLE 5. KS TESTS' RESULTS CUMULATIVE RESULTS FOR BEST DISTRIBUTION FIT (I, P, B FRAMES SEPARATELY)

distribution	results per distribution
exponential	3.5%
gamma	25.5%
lognormal	24%
weibull	28%
pearsonV	13%
geometric	4%
negative binomial	2%

TABLE 6. KS TEST'S RESULTS FOR BEST DISTRIBUTION FIT FOR EACH VIDEO FRAME TYPE

distribution	results per distribution I frames	results per distribution P frames	results per distribution B frames
exponential	0%	2%	8%
gamma	25%	37%	16%
lognormal	17%	25%	30%
weibull	31%	29%	23%
pearsonV	23%	3.5%	12%
geometric	0%	2%	10%
negative binomial	3.5%	1.5%	1%

TABLE 7. KL TESTS' RESULTS CUMULATIVE RESULTS FOR BEST DISTRIBUTION FIT (I, P, B FRAMES SEPARATELY)

distribution	results per distribution
exponential	0%
gamma	0%
lognormal	2%
weibull	0%
pearsonV	98%
geometric	0%
negative binomial	0%

TABLE 8. KL TESTS' RESULTS FOR BEST DISTRIBUTION FIT FOR EACH VIDEO FRAME TYPE

distribution	results per distribution I frames	results per distribution P frames	results per distribution B frames
exponential	0%	0%	0%
gamma	0.5%	0%	0%
lognormal	1%	2%	2%
weibull	0%	0%	0%
pearsonV	98%	98%	98%
geometric	0%	0%	0%
negative binomial	0.5%	0%	0%

2.4. Finding the best fits

Although the fitting results when modeling each video frame type separately were clearly better than the results produced by modeling the whole sequence uniformly, the autocorrelation among video frames can never be perfectly "captured" by a distribution generating frame sizes independently, according to a declared mean and standard deviation, and therefore none of the fitting attempts (including the Pearson V), as good as they might be, can achieve perfect accuracy. However, these results lead us to extend our work in order to build a DAR model, which inherently uses the autocorrelation coefficient of lag-1 in its estimation. The model will be shown to be able to often capture quite accurately the behavior of multiplexed H.264 videoconference movies, by generating frame sizes independently for I, P and B frames.

Still, for the DAR(1) model to work, the best distribution fit needs to be found. The most important conclusion that is derived from this first part of our work is that, contrary to the results in [18, 24], which focused on modeling videoconference traffic, the three statistical tests (Q-Q plot, KS test, KL test) used in our study **do not** agree, in many cases, on which distribution provides the best fit (in [18, 24] in almost all the cases examined, the three tests provided identical results). The reason is the much lower autocorrelation of the H.264 video traces, compared with the high autocorrelation of H.263 and H.264 videoconference traffic. This lower autocorrelation (respective results will be presented in Section 3) makes the differences in frame sizes between successive frames larger, and hence makes the behavior of the trace more unpredictable. This fact, combined with the very different nature of the three statistical tests used in our study is responsible for their different "verdicts". More specifically, the Q-Q plot is of a qualitative nature and is based on observation; therefore, in the case when different distributions provide similar fitting results, the Q-Q plot can not provide a definite conclusion on which distribution is the best fit. On the other hand, the KS test does provide a quantitative result, but this concerns the maximum vertical deviation between two curves; therefore, it is clear which distribution has the minimum maximum distance from the "trace curve" but this is not conclusive in terms of whether this distribution also presents the closest fit.

For the above reasons, it could be argued that the KL test provides the most accurate information on the goodness-of-fit of a distribution, among the three tests.

In our work, in order to derive the best distribution fit for each case, we have used the following procedure: in the cases where all three statistical tests or two out of the three tests denoted the same distribution as the best fit, we have considered that distribution as the most suitable for use in our DAR model. In the cases where the three tests denoted different distributions as the best fit, we compared the results of the KL test with the results of the Q-Q plot test. If the distribution that was the best fit according to the KL test was a close second best according to the Q-Q plot test, then we used that distribution as the best fit. This was a case which we encountered in many of the traces under study. If this wasn't the case (i.e., all tests offered different results and the best KL fit was not shown to be a good fit by the Q-Q plot test), then the specific trace was not included in our DAR(1) modeling study which will be presented in Section 3. 24% of the traces were not included in our DAR(1) study because of this reason.

Table 9 presents the best fit results for all traces, based on the above-described methodology.

TABLE 9. BEST FIT FINAL RESULTS

distribution	results per distribution
exponential	0%
gamma	17%
lognormal	13%
weibull	23%
pearsonV	22%
geometric	0%
negative binomial	11%
all tests offered different results	24%

3. MODELING MULTIPLEXED H.264 VIDEO TRAFFIC

In this section we build a Discrete Autoregressive (DAR(1)) model with the purpose of "capturing" the behavior of multiplexed H.264 video traffic.

3.1. The DAR(1) Model

A Discrete Autoregressive model of order p, denoted as DAR(p), generates a stationary sequence of discrete random variables with an arbitrary probability distribution and with an autocorrelation structure similar to that of an Autoregressive model [14]. DAR(1) is a special case of a DAR(p) process and it is defined as follows: let $\{V_n\}$ and $\{Y_n\}$ be two sequences of independent random variables. The random variable V_n can take two values, 0 and 1, with probabilities 1-ρ and ρ, respectively. The random variable Y_n has a discrete state S and $P\{Y_n=i\}=\pi(i)$. The sequence of random variables $\{X_n\}$ which is formed according to the linear model:

$$X_n=V_nX_{n-1}+(1-V_n)Y_n \qquad (1)$$

is a DAR(1) process.

A DAR(1) process is a Markov chain with discrete state space S and transition matrix:

$$P=\rho I+(1-\rho)Q \qquad (2)$$

where ρ is the autocorrelation coefficient, I is the identity matrix and Q is a matrix with $Q_{ij}=\pi(j)$ for i,j in S.

Autocorrelations are usually plotted for a range W of lags. The autocorrelation can be calculate by the formula:

$$\rho(W)=\frac{E[(Xi-\mu)(Xi+w-\mu)]}{\sigma^2} \qquad (3)$$

where μ is the mean and σ^2 the variance of the frame size for a specific video trace.

As in [5], where a DAR(1) model with negative binomial distribution (i.e., the best distribution fit) was used to model the number of cells per frame of VBR teleconferencing video, we want to build a model based only on parameters which are either known at call set-up time or can be measured without introducing much complexity in the network. DAR(1) provides an easy and practical method to compute the transition matrix and gives us a model based only on four physically meaningful parameters, i.e., the mean, peak, variance and the lag-1 autocorrelation coefficient ρ of the offered traffic. The DAR(1) model can be used with any marginal distribution [22].

We proceeded to build a DAR(1) model for each one of the traces under study. More specifically, in our model the rows of the Q matrix consist of the "best" distribution probabilities (f_0, f_1,…, f_k, f_K), where $F_K=\Sigma_{k>K}f_k$, and K is the peak rate. Each k, for k<K, corresponds to possible source rates less than the peak rate of K.

From the transition matrix in (2) it is evident that if the current frame has, for example, i cells, then the next frame will have i cells with probability $\rho+(1-\rho)f_i$, and will have k cells, $k\neq i$, with probability $(1-\rho)f_k$. Therefore the number of cells per video frame stays constant from one (I, P or B) video frame to the next (I, P or B) video frame, respectively, in our model with a probability slightly larger than ρ.

The Markov chain generated by the DAR(1) model is presented in Figure 9. The number of a state is essentially the number of video packets per frame. Each packet contains 48 bytes. Thus, the maximum number of packets that can be generated from the model results by dividing the largest video frame size of the actual trace under study with the number 48.

The autocorrelation coefficient of lag-1 is calculated for all types of video frames of the movies, using the formula (3) with w=1, as it shows the degree of correlation between successive frames of the same type. We also calculated the autocorrelation coefficient with lag-2 and with lag equal to the size of the GoP (lag-12 or lag-16), for each type of video frame as well as for the whole trace, for all traces under study. When studying the whole trace, the autocorrelation coefficient was found to be low for lag-1 and lag-2 and very high for lag equal to the size of GOP, showing the strong periodicity in video frame sizes between consecutive GOPs. When we studied each type of frame separately, the autocorrelation coefficient was often very high for lag-1, slightly lower for lag-2 and even lower (but still non-negligible) for lag equal to the size of GOP. Some indicative results are presented in appendix B. The autocorrelation for the whole NBC News (G16B7 QP28) trace and the I, P, B frames of the trace separately is shown in Figures 10a, 10b, 10c and 10d.

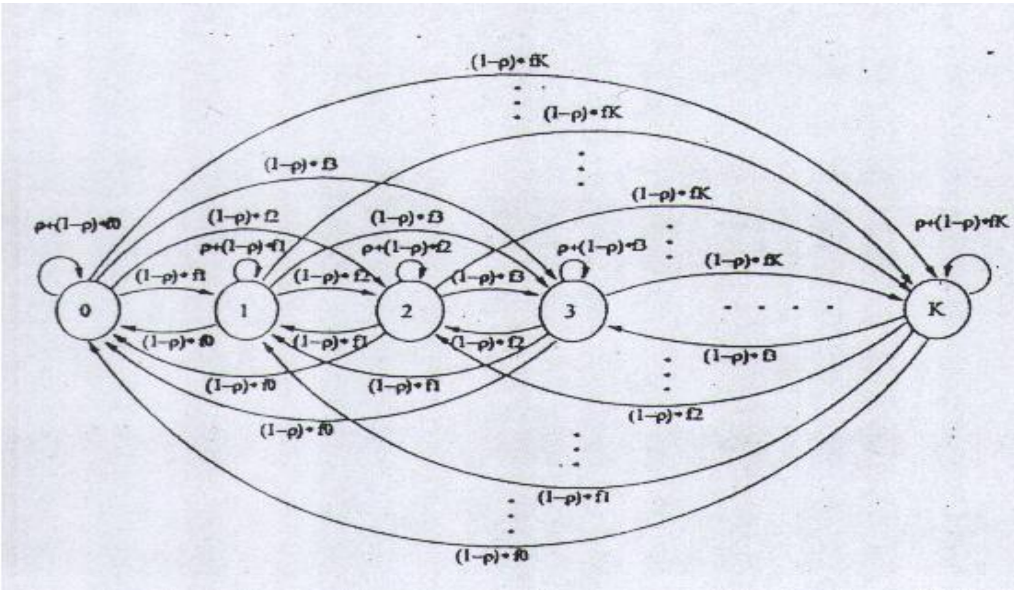

Figure 9. Markov chain generated from the DAR(1) model.

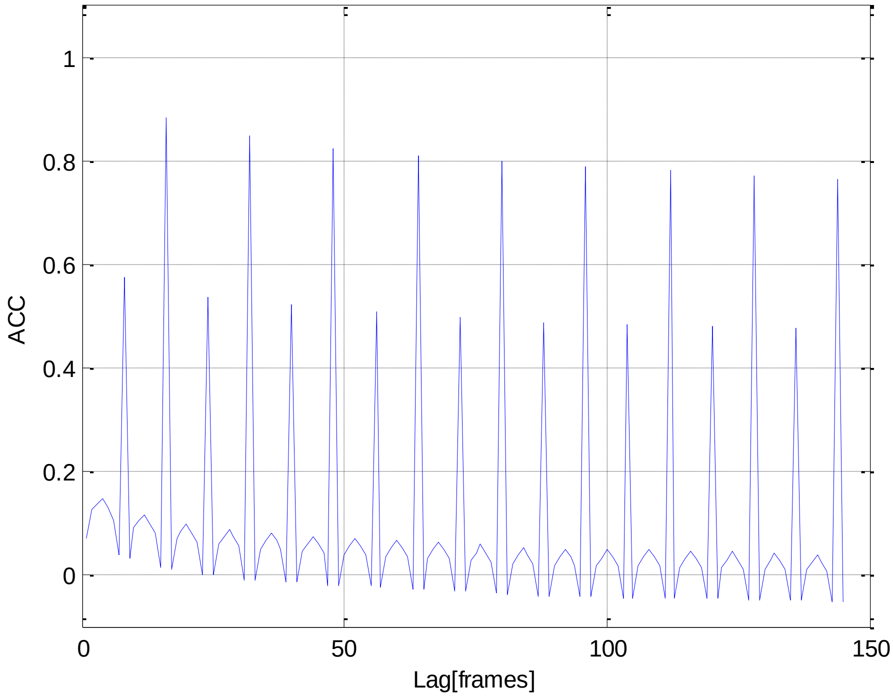

Figure 10a. Autocorrelation Coefficients for the whole NBC News trace ([G16, B7, QP28]).

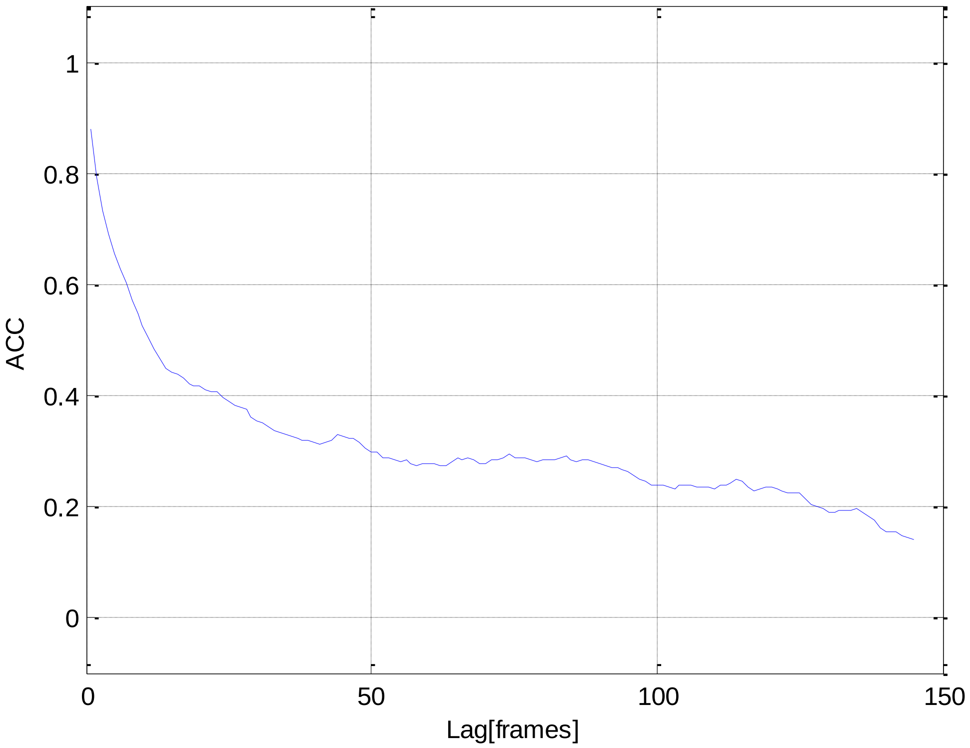

Figure 10b. Autocorrelation for the I frames of the NBC News trace ([G16, B7, QP28]).

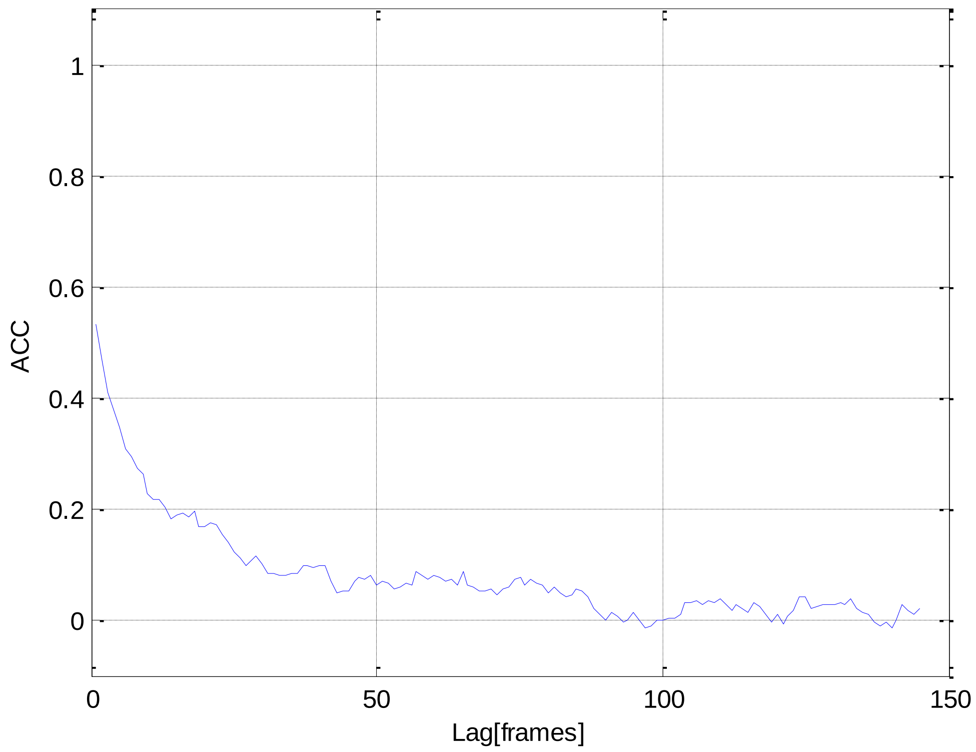

Figure 10c. Autocorrelation for the P frames of the NBC News trace ([G16, B7, QP28]).

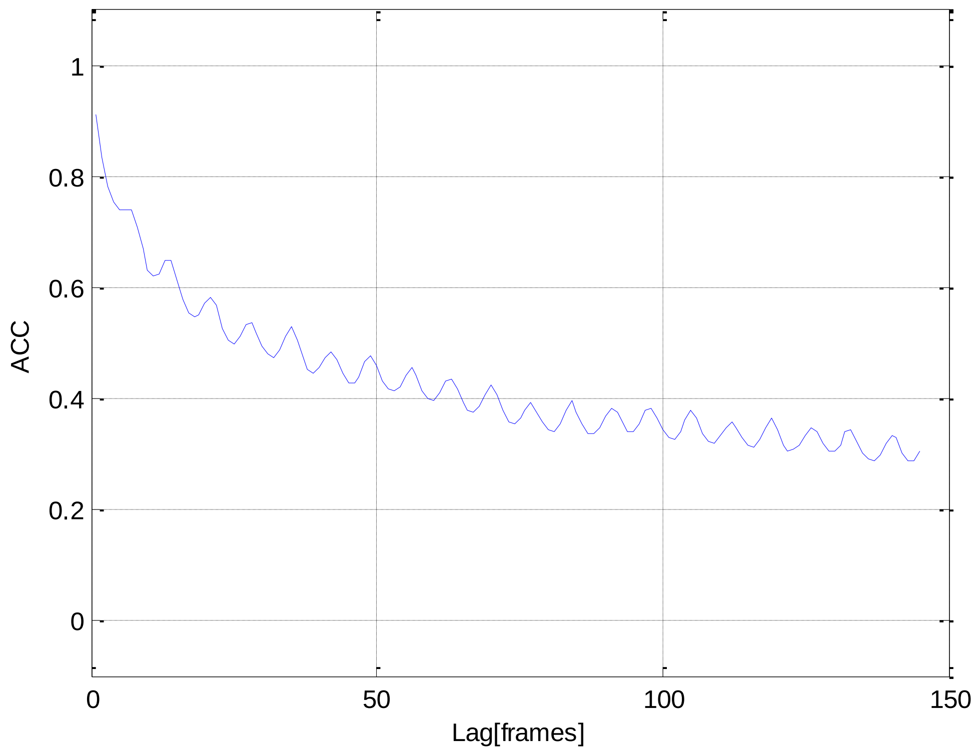

Figure 10d. Autocorrelation for the B frames of the NBC News trace ([G16, B7, QP28]).

3.2. Modeling results and discussion based on Q-Q plots

We proceeded with testing our model statistically in order to study whether it produces a good fit for the I, P, B frames for the trace superposition. For this reason we have used again Q-Q plots and we present indicatively some of these results in appendix B.

Our results have shown that the points of the Q-Q plots fall, in many but not all the cases under study, along the 45-degree reference line, with the exception of the last quantiles (right-hand tail). The very good fit in these cases (which correspond to 72% of the total traces used in our DAR(1) modeling study) shows that the superposition of the actual traces can be modeled very well by a respective superposition of data produced by the DAR(1) model. In the cases where the DAR(1) model does not provide satisfactory results, this was caused by the lack of an accurate distribution fit, as explained in the first part of our work.

From the results presented in Appendix B, it is clear that in most cases, as the number of sources increases, the modeling results are better (the authors in [5, 18, 24] have reached similar conclusions for their own DAR(1) models and they present results for a superposition of 5-20 traces).

In the cases, however, where the initial distribution fit is not accurate, it can happen that the DAR(1) model for a superposition of 5 traces is better than the respective model for a superposition of 15 traces; the reason is that the poor initial modeling results lead to greater differences between the model and the actual data as the number of sources increases. Such an example is shown in Figure AB33, in Appendix B.

4. CONCLUSIONS

Models of video traffic are very important, as networks need to handle video traffic competently (i.e. to guarantee its strict QoS requirements despite its burstiness). Hence in this work we have investigated the subject of modeling H.264 video traffic.

We have investigated the possibility of modeling a large number (close to 200) single H.264 video traces with well-known distributions. The results showed that there is not one distribution that is most suitable for all traces, but rather that the best distribution fit depends on the trace.

Our approach was to model separately the I, P and B frames of each trace, in order to achieve better modeling accuracy. Our results have shown that this is a clearly better choice than modeling the whole trace; however, the behavior of video traffic can never be perfectly "captured" by a distribution generating independently frame sizes according to a declared mean and standard deviation, due to the autocorrelation of video traffic. Hence, none of the fitting attempts can achieve high accuracy.

We used the fitting results in order to build a simple DAR(1) model (separately for I, P and B frames) to capture the behavior of multiplexed H.264 video sources. The DAR(1) model was shown to provide various degrees of modeling accuracy, but in many cases succeeded in providing a highly accurate model for multiplexed H.264 videos. The simplicity of the model makes it a good candidate for modeling video traffic for networking purposes, as it demands low implementation complexity in comparison to wavelet approaches such as [12] which can offer higher accuracy at the cost of significantly higher complexity.

The results of this work have been used in [25, 26], in the study of the FPRRA framework for video traffic transmission over GEO satellites.

REFERENCES

[1] S. M. Cherry, “Fiber to the home”, IEEE Spectrum, Vol. 41, No. 1, 2004, pp. 42-43.

[2] M. Etoh and T. Yoshimura, “Advances in Wireless Video Delivery”, Proc. of the IEEE, Vol. 93, No. 1, 2005, pp. 111-122.

[3] D. M. Lucantoni, M. F. Neuts and A. R. Reibman, “Methods for Performance Evaluation of VBR Video Traffic Models,” IEEE/ACM Trans. Networking, Vol. 2, 1994, pp. 176-180.

[4] M. Nomura, T. Fuji and N. Ohta, “Basic Characteristics of Variable Rate Video Coding in ATM Environment”, IEEE Journal on Selected Areas in Communications, Vol. 7, No. 5, 1989, pp. 752-760.

[5] D. P. Heyman, A. Tabatabai and T. V. Lakshman, “Statistical Analysis and Simulation Study of Video Teleconference Traffic in ATM Networks”, IEEE Trans. on Circuits and Systems for Video Technology, Vol. 2, No. 1, 1992, pp. 49-59.

[6] A. M. Dawood and M. Ghanbari, “Content-based MPEG Video Traffic Modeling”, IEEE Trans. on Multimedia, Vol. 1, No. 1, 1999.

[7] B. Melamed and D. E. Pendarakis, “Modeling Full-Length VBR Video Using Markov-Renewal Modulated TES Models”, IEEE Journal on Selected Areas in Communications, Vol. 16, No. 5, 1998, pp. 600-611.

[8] K. Chandra and A. R. Reibman, “Modeling One- and Two-Layer Variable Bit Rate Video”, IEEE/ACM Trans. on Networking, Vol. 7, No. 3, 1999, pp. 398-413.

[9] D. P. Heyman, “The GBAR Source Model for VBR Videoconferences”, IEEE/ACM Trans. on Networking, Vol. 5, No. 4, 1997.

[10] M. Frey and S. Ngyuyen-Quang, "A Gamma-Based Framework for Modeling Variable-Rate Video Sources: The GOP GBAR Model", IEEE/ACM Trans. on Networking, Vol. 8, No. 6, 2000, pp. 710-719.

[11] S. Kempken and W. Luther, "Modeling of H.264 High Definition Video Traffic Using Discrete-Time Semi-Markov Processes", in Proc. of ITC 2007, Lecture Notes in Computer Science (LNCS) Vol. 4516, 2007, pp. 42–53.

[12] M. Dai, Y. Zhang and D. Loguinov, "A Unified Traffic Model for MPEG-4 and H.264 Video Traces", IEEE Transactions on Multimedia, Vol. 11, No. 5, 2009, pp. 1010-1023.

[13] I. Reljin, A. Samcovic and B. Reljin, "H.264/AVC Video Compressed Traces: Multifractal and Fractal Analysis", EURASIP Journal on Applied Signal Processing, Vol. 2006, Issue 1, 2006, pp. 1-12.

[14] P. A. Jacobs and P. A. W. Lewis, "Time Series Generated by Mixtures", Journal of Time Series Analysis, Vol. 4, No. 1, 1983, pp. 19-36.

[15] U. K. Sarkar, S. Ramakrishnan and D. Sarkar, "Modeling Full-Length Video Using Markov-Modulated Gamma-Based Framework," IEEE/ACM Trans. on Networking, Vol. 11, No.4, 2003, pp. 638-649.

[16] D. Marpe, T. Wiegand and G. Sullivan, "The H.264/MPEG4 Advanced Video Coding Standard and its Applications", IEEE Communications Magazine, vol. 44, no. 8, Aug. 2006, pp. 134–143.

[17] G. Van der Auwera, P. David and M. Reisslein, "Traffic and Quality Characterization of Single-Layer Video Streams Encoded with the H.264/MPEG-4 Advanced Video Coding Standard and Scalable Video Coding Extension", IEEE Trans. on Broadcasting, Vol. 54, No. 3, September 2008, pp. 698-718.

[18] P. Koutsakis, “A New Model for Multiplexed VBR H.263 Videoconference Traffic”, in Proc. of the IEEE GLOBECOM 2006.

[19] [Online] http://trace.eas.asu.edu/hd/index.html

[20] A. M. Law and W. D. Kelton, “Simulation Modeling & Analysis”, 2nd Ed., McGraw Hill Inc., 1991.

[21] K. P. Burnham and D. R. Anderson, “Model Selection and Multi-Model Inference”, Springer-Verlag, New York, 2002.

[22] T. V. Lakshman, A. Ortega and A. R. Reibman, “VBR Video: Trade-offs and potentials”, Proc. of the IEEE, Vol. 86, No. 5, 1998.

[23] M. Krunz and H. Hughes, “A Traffic Model for MPEG-coded VBR Streams”, in Proc. of the ACM SIGMETRICS 1995, pp. 47-55.

[24] A. Lazaris and P. Koutsakis, “Modeling Multiplexed Traffic from H.264/AVC Videoconference Streams”, Computer Communications Journal, Vol. 33, No. 10, 2010, pp. 1235-1242.

[25] P. Koutsakis, D. Vasileiadou and C. Stamos, “Performance Evaluation of the FPRRA Framework for GEO Satellites in the Absence of Accurate Multimedia Traffic Prediction”, invited paper to the inaugural issue of the International Journal on Communications, Antenna and Propagation (Praise Worthy Prize Publishing), February 2011.

[26] P. Koutsakis, C. Stamos, D. Vasileiadou and A. Lazaris, “Performance Evaluation of the FPRRA Framework for GEO Satellites in the Absence of Accurate Video Traffic Modeling”, accepted for presentation in the 1st IEEE International Conference on Consumer Electronics-Berlin 2011, September 2011.

APPENDIX A

In this appendix we present the date for the peak, mean and standard deviation of the traces which were used in our study.

	trace	Peak (Bytes)	Mean (Bytes)	Standard deviation (Bytes)
1	Tokyo Olympics G16B1 QP10	95219	15259	10934
2	Tokyo Olympics G16B1 QP16	62269	7004	6595
3	Tokyo Olympics G16B1 QP22	40151	2897	3661
4	Tokyo Olympics G16B1 QP24	35451	2192	2975
5	Tokyo Olympics G16B1 QP28	27652	1326	2005
6	Tokyo Olympics G16B1 QP34	17313	635	1059
7	Tokyo Olympics G16B1 QP38	11140	388	654
8	Tokyo Olympics G16B1 QP42	6629	239	397
9	Tokyo Olympics G16B1 QP48	2017	112	175
10	Tokyo Olympics G16B3 QP10	95566	15472	9757
11	Tokyo Olympics G16B3 QP16	62469	6773	6272
12	Tokyo Olympics G16B3 QP22	40362	2803	3586
13	Tokyo Olympics G16B3 QP24	35695	2121	2932
14	Tokyo Olympics G16B3 QP28	27850	1274	1989
15	Tokyo Olympics G16B3 QP34	17429	601	1062
16	Tokyo Olympics G16B3 QP38	11292	365	660
17	Tokyo Olympics G16B3 QP42	6752	221	402
18	Tokyo Olympics G16B3 QP48	2034	101	178
19	Tokyo Olympics G16B7 QP10	96634	16254	9010

20	Tokyo Olympics G16B7 QP16	63389	7145	6049
21	Tokyo Olympics G16B7 QP22	40814	3024	3571
22	Tokyo Olympics G16B7 QP24	36154	2297	2937
23	Tokyo Olympics G16B7 QP28	28338	1375	1993
24	Tokyo Olympics G16B7 QP34	17953	639	1066
25	Tokyo Olympics G16B7 QP38	11752	384	668
26	Tokyo Olympics G16B7 QP42	7122	227	4082
27	Tokyo Olympics G16B7 QP48	2248	98	179
28	Tokyo Olympics G16B15 QP10	97496	17242	8669
29	Tokyo Olympics G16B15 QP16	64336	7758	5989
30	Tokyo Olympics G16B15 QP22	41313	3413	3637
31	Tokyo Olympics G16B15 QP24	36664	2617	3010
32	Tokyo Olympics G16B15 QP28	28816	1583	2038
33	Tokyo Olympics G16B15 QP34	18410	732	1079
34	Tokyo Olympics G16B15 QP38	12244	435	673
35	Tokyo Olympics G16B15 QP42	7539	248	407
36	Tokyo Olympics G16B15 QP48	2738	99	117
37	Silence of the Lambs G16B1 QP10	81734	7885	8683
38	Silence of the Lambs G16B1 QP16	51655	3097	4804
39	Silence of the Lambs G16B1 QP22	35533	1361	2631
40	Silence of the Lambs G16B1 QP24	30838	1041	2130
41	Silence of the Lambs G16B1 QP28	23015	633	1414
42	Silence of the Lambs G16B1 QP34	13046	306	723
43	Silence of the Lambs G16B1 QP38	8143	190	438

44	Silence of the Lambs G16B1 QP42	4746	121	262
45	Silence of the Lambs G16B1 QP48	1821	64	117
46	Silence of the Lambs G16B3 QP10	82228	7430	8416
47	Silence of the Lambs G16B3 QP16	51991	2947	4733
48	Silence of the Lambs G16B3 QP22	35814	1296	2613
49	Silence of the Lambs G16B3 QP24	31061	991	2122
50	Silence of the Lambs G16B3 QP28	23198	601	1410
51	Silence of the Lambs G16B3 QP34	13203	287	722
52	Silence of the Lambs G16B3 QP38	8291	177	439
53	Silence of the Lambs G16B3 QP42	4857	112	263
54	Silence of the Lambs G16B3 QP48	1870	59	118
55	Silence of the Lambs G16B7 QP10	83620	7707	8246
56	Silence of the Lambs G16B7 QP16	53002	3102	4738
57	Silence of the Lambs G16B7 QP22	36404	1377	2653
58	Silence of the Lambs G16B7 QP24	31696	1051	2162
59	Silence of the Lambs G16B7 QP28	23775	634	1440
60	Silence of the Lambs G16B7 QP34	13688	297	737
61	Silence of the Lambs G16B7 QP38	8662	182	449
62	Silence of the Lambs G16B7 QP42	5130	112	268
63	Silence of the Lambs G16B7 QP48	1974	57	119
64	Silence of the Lambs G16B15 QP10	85012	8390	8173
65	Silence of the Lambs G16B15 QP16	54191	3442	4773
66	Silence of the Lambs G16B15 QP22	37080	1554	2707
67	Silence of the Lambs G16B15 QP24	32396	1189	2214

68	Silence of the Lambs G16B15 QP28	24440	713	1475
69	Silence of the Lambs G16B15 QP34	14204	327	755
70	Silence of the Lambs G16B15 QP38	9169	197	459
71	Silence of the Lambs G16B15 QP42	5533	118	272
72	Silence of the Lambs G16B15 QP48	2148	55	117
73	Star Wars IV G16B1 QP10	52381	7292	7253
74	Star Wars IV G16B1 QP16	31463	3103	4075
75	Star Wars IV G16B1 QP22	18919	1433	2222
76	Star Wars IV G16B1 QP24	15356	1105	1794
77	Star Wars IV G16B1 QP28	10452	678	1183
78	Star Wars IV G16B1 QP34	6403	329	616
79	Star Wars IV G16B1 QP38	4290	204	385
80	Star Wars IV G16B1 QP42	2951	131	244
81	Star Wars IV G16B1 QP48	1729	71	122
82	Star Wars IV G16B3 QP10	52977	6783	7152
83	Star Wars IV G16B3 QP16	32681	2976	4062
84	Star Wars IV G16B3 QP22	19106	1382	2225
85	Star Wars IV G16B3 QP24	15596	1063	1800
86	Star Wars IV G16B3 QP28	10500	648	1189
87	Star Wars IV G16B1 QP34	6474	311	620
88	Star Wars IV G16B3 QP38	4339	194	388
89	Star Wars IV G16B3 QP42	2957	124	246
90	Star Wars IV G16B3 QP48	1730	67	122
91	Star Wars IV G16B7 QP10	50652	6939	6882

92	Star Wars IV G16B7 QP16	32157	3105	4003
93	Star Wars IV G16B7 QP22	19584	1460	2230
94	Star Wars IV G16B7 QP24	16011	1123	1808
95	Star Wars IV G16B7 QP28	10674	681	1200
96	Star Wars IV G16B7 QP34	6599	323	628
97	Star Wars IV G16B7 QP38	4437	201	394
98	Star Wars IV G16B7 QP42	3066	128	248
99	Star Wars IV G16B7 QP48	1823	67	122
100	Star Wars IV G16B15 QP10	47856	7618	6589
101	Star Wars IV G16B15 QP16	32767	3460	3870
102	Star Wars IV G16B15 QP22	20075	1656	2213
103	Star Wars IV G16B15 QP24	16437	1279	1808
104	Star Wars IV G16B15 QP28	10877	769	1210
105	Star Wars IV G16B15 QP34	6805	359	636
106	Star Wars IV G16B15 QP38	4603	221	400
107	Star Wars IV G16B15 QP42	3144	138	250
108	Star Wars IV G16B15 QP48	1632	69	119
109	Sony Demo G16B1 QP10	104148	16635	14420
110	Sony Demo G16B1 QP16	65552	8259	9446
111	Sony Demo G16B1 QP22	43608	3890	5931
112	Sony Demo G16B1 QP24	37670	2959	4946
113	Sony Demo G16B1 QP28	27708	1758	3429
114	Sony Demo G16B1 QP34	16086	786	1824
115	Sony Demo G16B1 QP38	10492	449	1107

116	Sony Demo G16B1 QP42	6638	262	653
117	Sony Demo G16B1 QP48	2887	119	270
118	Sony Demo G16B3 QP10	104112	16273	14113
119	Sony Demo G16B3 QP16	66242	7926	9257
120	Sony Demo G16B3 QP22	43808	3580	5909
121	Sony Demo G16B3 QP24	37882	2702	4961
122	Sony Demo G16B3 QP28	27861	1600	3469
123	Sony Demo G16B3 QP34	16233	728	1855
124	Sony Demo G16B3 QP38	10579	422	1128
125	Sony Demo G16B3 QP42	6734	248	666
126	Sony Demo G16B3 QP48	2904	110	257
127	Sony Demo G16B7 QP10	101206	17039	13990
128	Sony Demo G16B7 QP16	65289	8353	176
129	Sony Demo G16B7 QP22	44458	3773	5883
130	Sony Demo G16B7 QP24	38480	2831	4964
131	Sony Demo G16B7 QP28	28460	1641	3506
132	Sony Demo G16B7 QP34	16725	742	1907
133	Sony Demo G16B7 QP38	10947	436	1171
134	Sony Demo G16B7 QP42	7108	255	697
135	Sony Demo G16B7 QP48	3185	112	286
136	Sony Demo G16B15 QP10	102765	18618	14023
137	Sony Demo G16B15 QP16	66670	9296	84194096
138	Sony Demo G16B15 QP22	45228	4296	5926
139	Sony Demo G16B15 QP24	39202	3245	5013

140	Sony Demo G16B15 QP28	29162	1857	3542
141	Sony Demo G16B15 QP34	17190	806	1950
142	Sony Demo G16B15 QP38	11376	470	1215
143	Sony Demo G16B15 QP42	7471	274	731
144	Sony Demo G16B15 QP48	3528	116	301
145	NBC News G16B1 QP10	88254	29108	9808
146	NBC News G16B1 QP16	56417	13367	7788
147	NBC News G16B1 QP22	36027	4949	4840
148	NBC News G16B1 QP24	30995	3535	3970
149	NBC News G16B1 QP28	22637	1976	2713
150	NBC News G16B1 QP34	13948	889	1472
151	NBC News G16B1 QP38	9756	528	934
152	NBC News G16B1 QP42	6703	321	586
153	NBC News G16B1 QP48	3504	149	277
154	NBC News G16B3 QP10	90775	27584	9508
155	NBC News G16B3 QP16	59352	12351	7453
156	NBC News G16B3 QP22	36217	4530	4787
157	NBC News G16B3 QP24	31148	3270	3941
158	NBC News G16B3 QP28	22815	1828	2703
159	NBC News G16B3 QP34	14141	822	1478
160	NBC News G16B3 QP38	9853	493	941
161	NBC News G16B3 QP42	6756	298	591
162	NBC News G16B3 QP48	3527	135	279
163	NBC News G16B7 QP10	93192	27439	9053

164	NBC News G16B7 QP16	60723	12397	7200
165	NBC News G16B7 QP22	36839	4629	4715
166	NBC News G16B7 QP24	31796	3366	3913
167	NBC News G16B7 QP28	23359	1885	2701
168	NBC News G16B7 QP34	14434	839	1493
169	NBC News G16B7 QP38	10121	505	961
170	NBC News G16B7 QP42	6988	303	604
171	NBC News G16B7 QP48	3721	131	284
172	NBC News G16B15 QP10	87785	27866	8555
173	NBC News G16B15 QP16	55876	12862	6801
174	NBC News G16B15 QP22	37657	4981	4600
175	NBC News G16B15 QP24	32475	3665	3850
176	NBC News G16B15 QP28	24034	2078	2670
177	NBC News G16B15 QP34	14882	919	1486
178	NBC News G16B15 QP38	10517	546	965
179	NBC News G16B15 QP42	7280	318	611
180	NBC News G16B15 QP48	3980	132	286
181	Terminator G12B2 QP10	405006	119212	52562
182	Terminator G12B2 QP22	159536	21189	17997
183	Terminator G12B2 QP28	90512	9227	9398
184	Terminator G12B2 QP34	49518	4538	5290
185	Terminator G12B2 QP38	30503	2922	3548
186	Terminator G12B2 QP42	21262	1955	2525
187	Terminator G12B2 QP48	14095	1052	1551

188	KAET's from Mars to Mars to China G12B2 QP28	326905	20207	30167
189	KAET's Horizon G12B2 QP28	100061	6394	11786
190	Sony Demo G12B2 QP10	499921	94961	78196
191	Sony Demo G12B2 QP22	211013	24181	31077
192	Sony Demo G12B2 QP28	132717	10231	18051
193	Sony Demo G12B2 QP34	77287	4629	9945
194	Sony Demo G12B2 QP38	49818	2814	6476
195	Sony Demo G12B2 QP42	31854	1820	4237
196	Sony Demo G12B2 QP48	17926	952	2262

APPENDIX B

In this appendix we present indicatively some of our results, based on Q-Q plots, of the DAR(1) model accuracy. We present 24 very accurate fitting results, 6 relatively accurate fitting results and 3 results with low accuracy.

Very accurate fitting results:

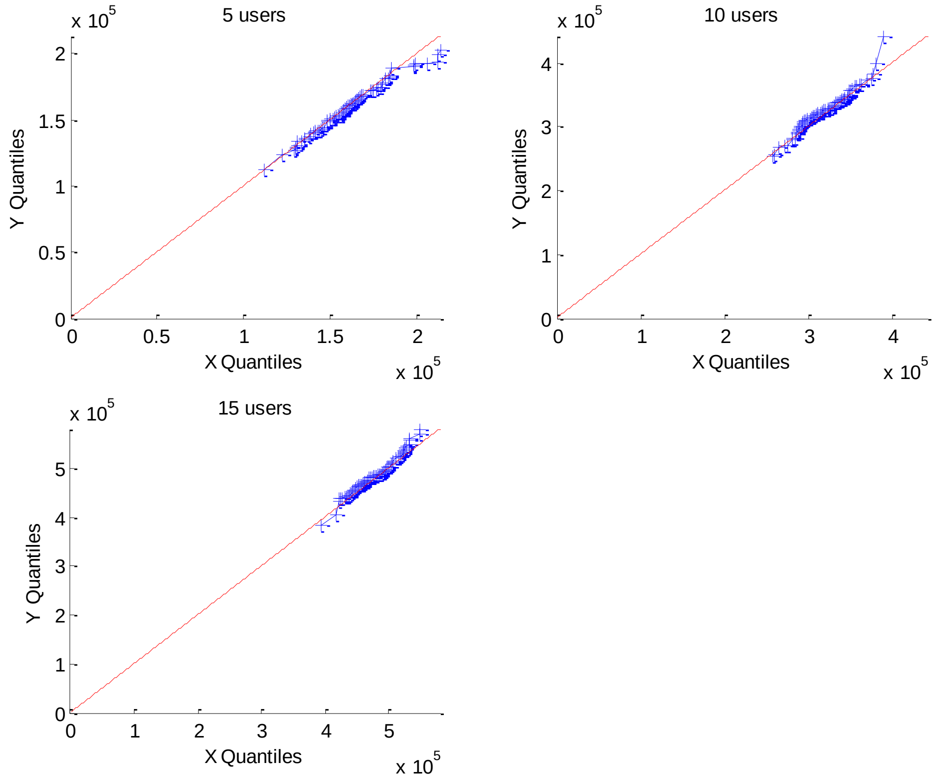

Figure AB1: Q-Q plot of the DAR(1) model versus the actual trace for the I frames of Terminator(G12B2 QP10), for 5, 10 and 15 superposed sources.

ACC1	0.86043
ACC2	0.76011
ACC16	0.257

Table AB1a: autocorrelation coefficient for the I frames of Terminator(G12B2 QP10).

ACC1	0.27956
ACC2	0.27379
ACC12	0.92055

Table AB1b: autocorrelation coefficient for the whole Terminator trace(G12B2 QP10).

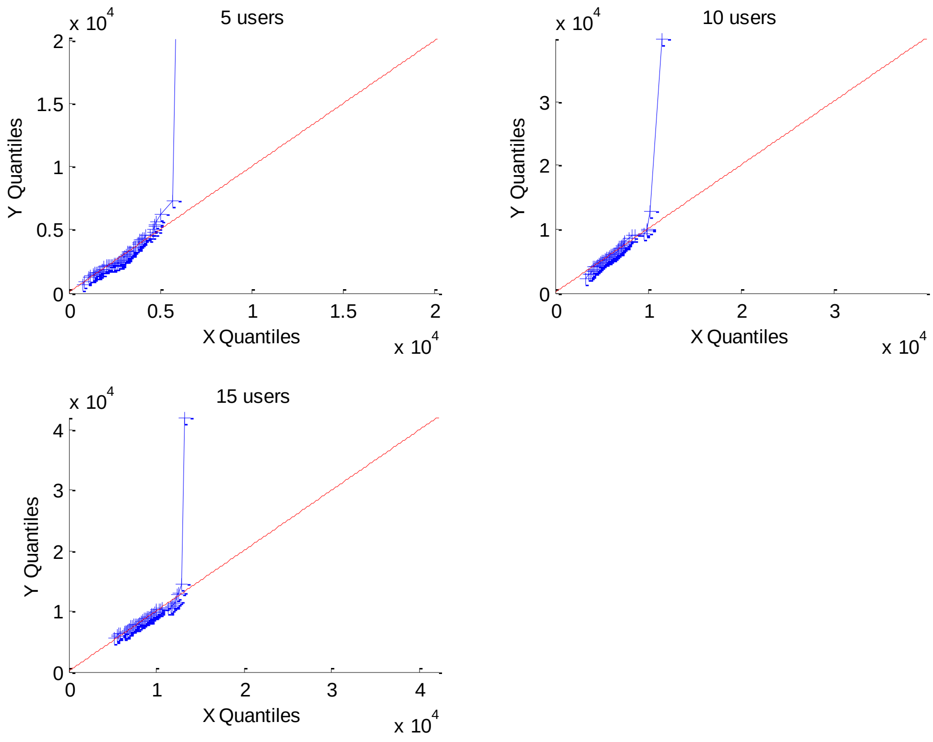

Figure AB2: Q-Q plot of the DAR(1) model versus the actual trace for the P frames of Sony Demo(G12B2 QP38), for 5, 10 and 15 superposed sources.

ACC1	0.65385
ACC2	0.74246
ACC16	0.66744

Table AB2a: autocorrelation coefficient for the P frames of Sony Demo(G12B2 QP38).

ACC1	-0.12831
ACC2	-0.1279
ACC12	0.97528

Table AB2b: autocorrelation coefficient for the whole Sony Demo trace(G12B2 QP38).

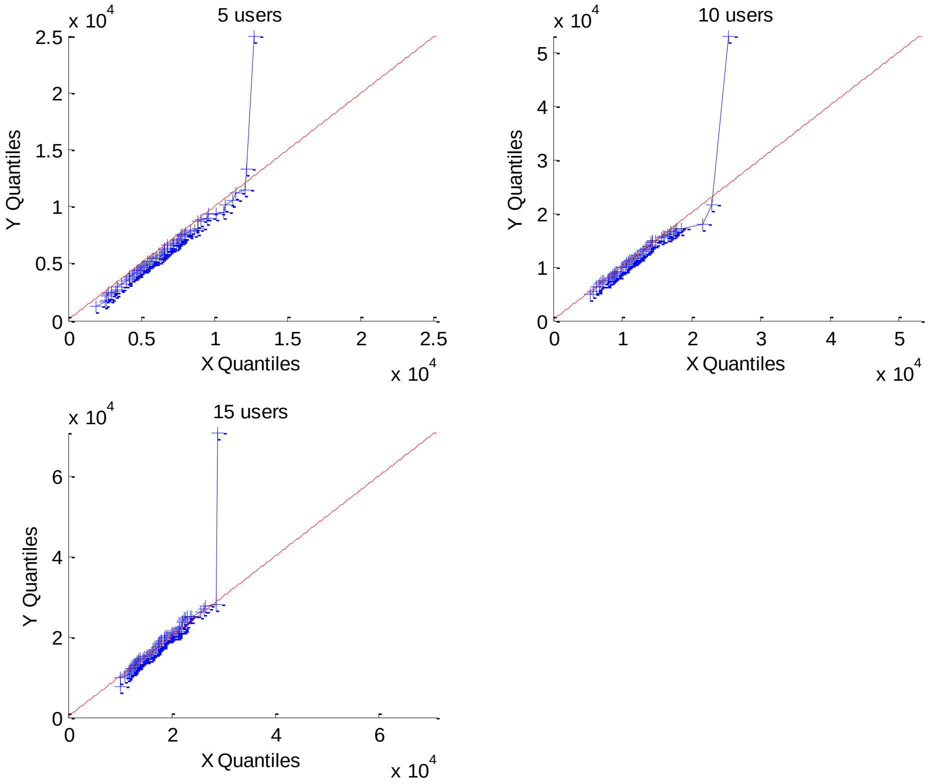

Figure AB3: Q-Q plot of the DAR(1) model versus the actual trace for the B frames of KAET's from Mars to China(G12B2 QP28), for 5, 10 and 15 superposed sources.

ACC1	0.94331
ACC2	0.91272
ACC16	0.74735

Table AB3a: autocorrelation coefficient for the B frames of KAET's from Mars to China (G12B2 QP28).

ACC1	-0.090679
ACC2	-0.09152
ACC12	0.95908

Table AB3b: autocorrelation coefficient for the whole KAET's from Mars to China trace(G12B2 QP28).

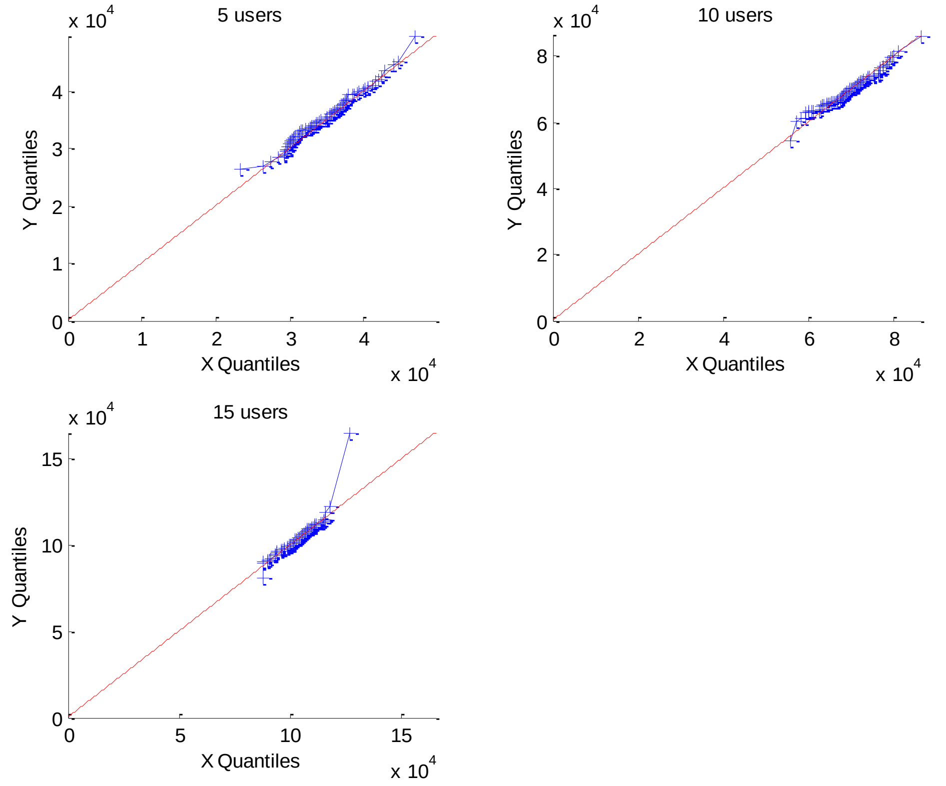

Figure AB4: Q-Q plot of the DAR(1) model versus the actual trace for the B frames of KAET's Horizon(G12B2 QP28), for 5, 10 and 15 superposed sources.

ACC1	0.93287
ACC2	0.86279
ACC16	0.37954

Table AB4a: autocorrelation coefficient for the B frames of KAET's Horizon(G12B2 QP28).

ACC1	-0.16073
ACC2	-0.16018
ACC12	0.98053

Table AB4b: autocorrelation coefficient for the whole KAET's Horizon trace(G12B2 QP28).

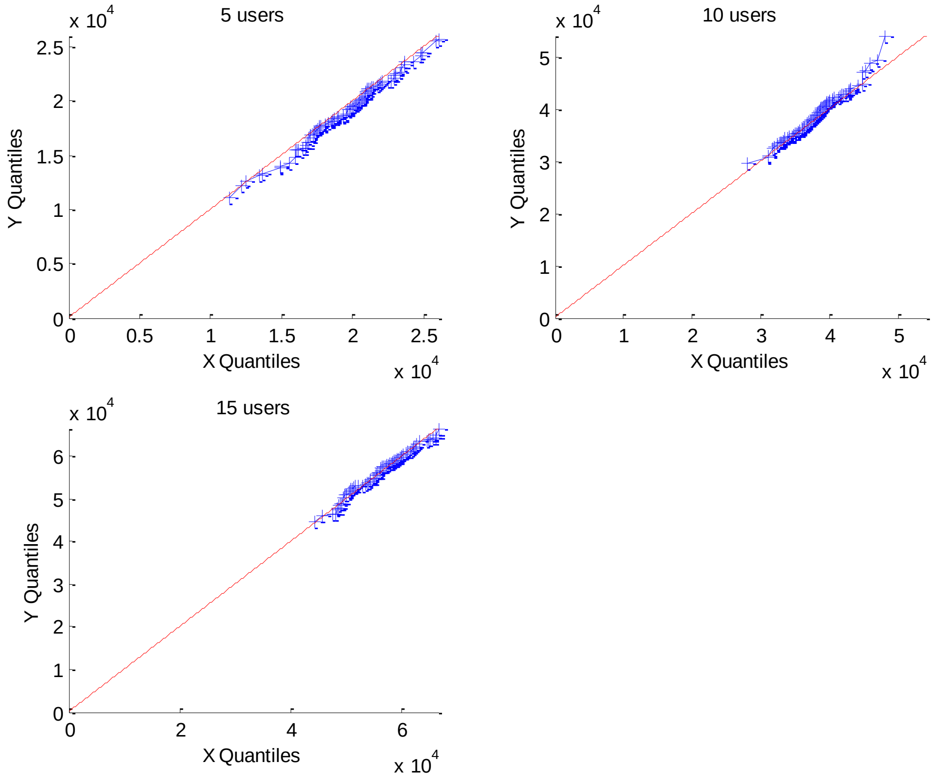

Figure AB5: Q-Q plot of the DAR(1) model versus the actual trace for the I frames of Star Wars IV(G16B1 QP10), for 5, 10 and 15 superposed sources.

ACC1	0.89746
ACC2	0.80795
ACC16	0.45366

Table AB5a: autocorrelation coefficient for the I frames of Star Wars IV(G16B1 QP10).

ACC1	-0.028273
ACC2	-0.017128
ACC16	0.94995

Table AB5b: autocorrelation coefficient for the whole Star Wars IV trace(G16B1 QP10).

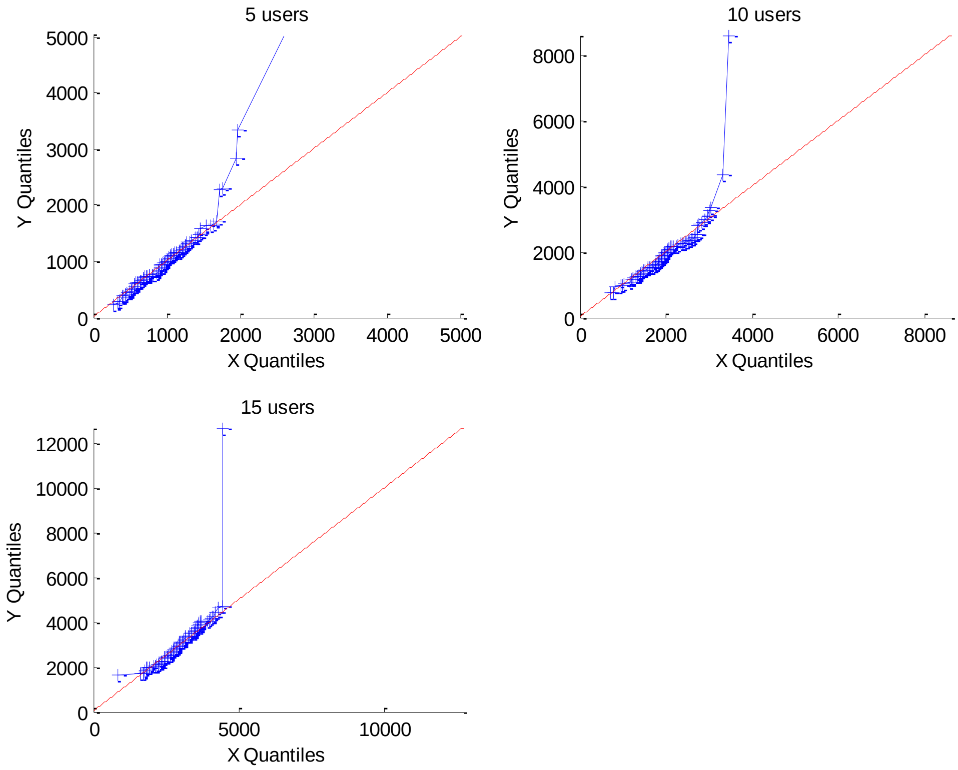

Figure AB6: Q-Q plot of the DAR(1) model versus the actual tarce for the P frames of Star Wars IV(G16B3 QP28), for 5, 10 and 15 superposed sources.

ACC1	0.63721
ACC2	0.58443
ACC16	0.31548

Table AB6a: autocorrelation coefficient for the P frames of Star Wars IV(G16B3 QP28).

ACC1	0.0026571
ACC2	0.042448
ACC16	0.88115

Table AB6b: autocorrelation coefficient for the whole Star Wars IV trace(G16B3 QP28).

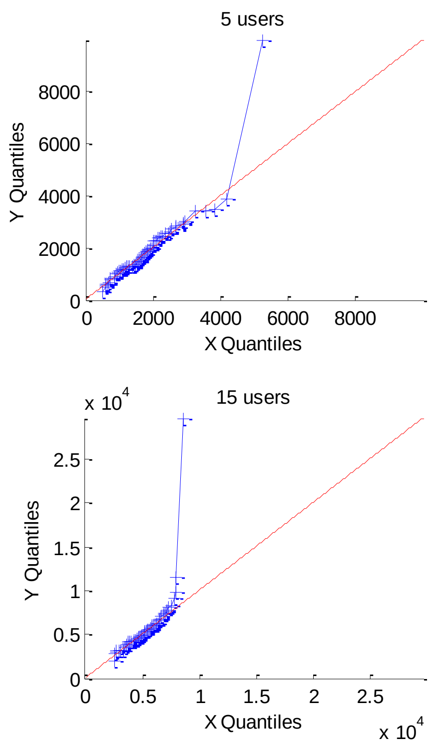

Figure AB7: Q-Q plot of the DAR(1) model versus the actual video for the B frames of Star Wars IV(G16B7 QP16), for 5, 10 and 15 superposed sources.

ACC1	0.92708
ACC2	0.86487
ACC16	0.67892

Table AB7a: autocorrelation coefficient for the B frames of Star Wars IV(G16B7 QP16).

ACC1	0.13855
ACC2	0.2067
ACC16	0.8765

Table AB7b: autocorrelation coefficient for the whole Star Wars IV trace(G16B7 QP16).

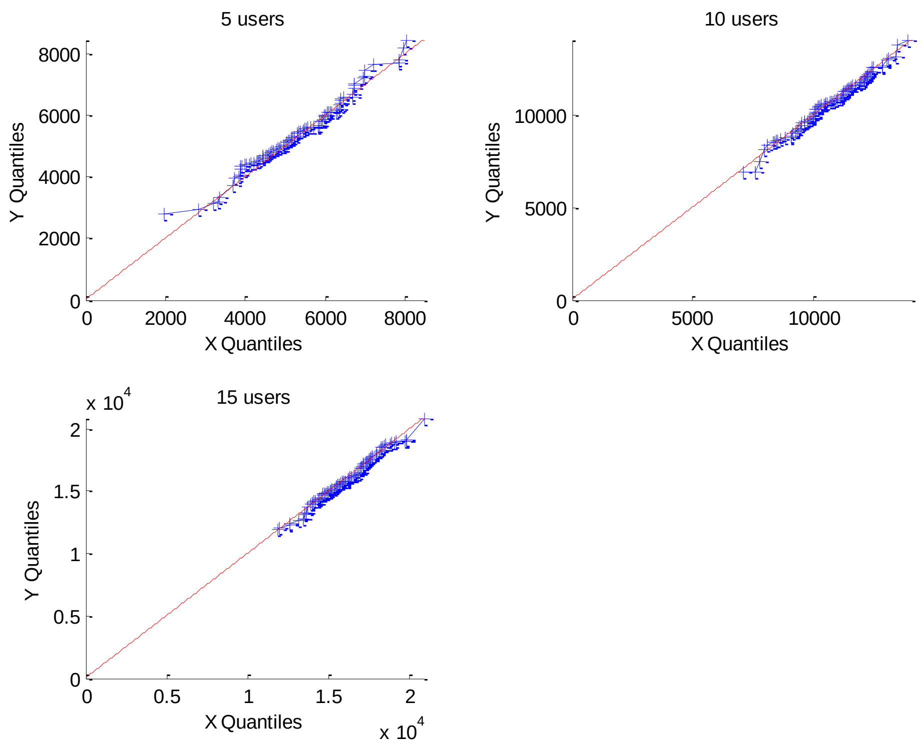

Figure AB8: Q-Q plot of the DAR(1) model versus the actual video for the P frames of Star Wars IV(G16B15 QP24), for 5, 10 and 15 superposed sources.

ACC1	0.89052
ACC2	0.79679
ACC16	0.4323

Table AB8a: autocorrelation coefficient for the P frames of Star Wars IV(G16B15 QP24).

ACC1	0.16519
ACC2	0.20687
ACC16	0.90635

Table AB8b: autocorrelation coefficient for whole Star Wars IV trace(G16B15 QP24).

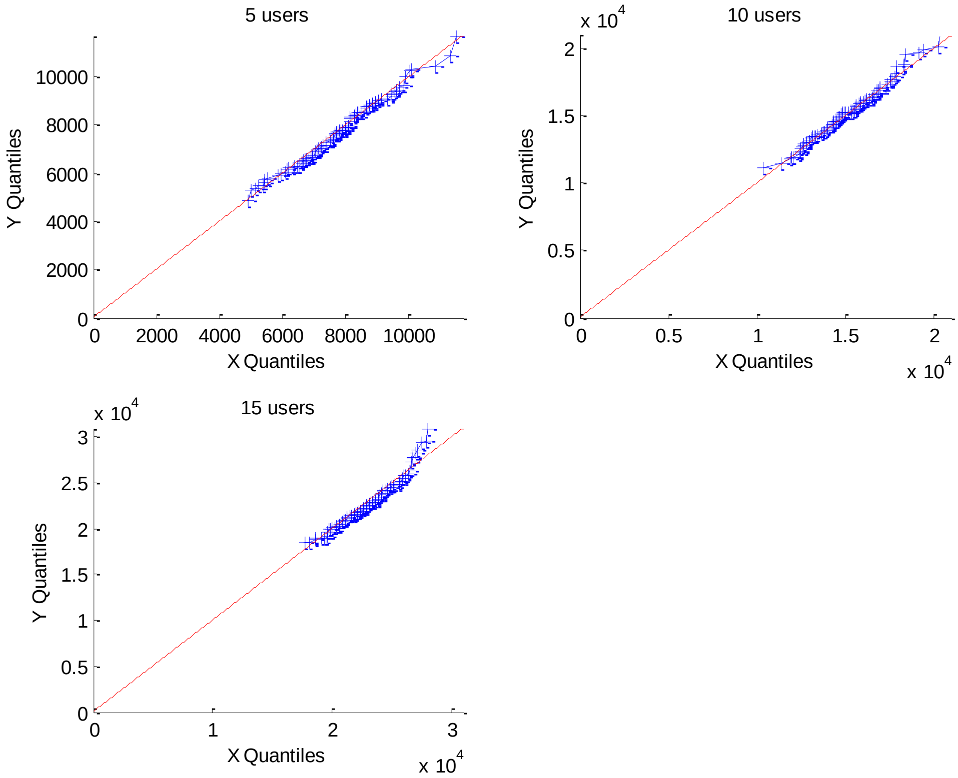

Figure AB9: Q-Q plot of the DAR(1) model versus the actual video for the I frames of NBC News(G16B1 QP28), for 5, 10 and 15 superposed sources.

ACC1	0.8799
ACC2	0.79327
ACC16	0.43741

Table AB9a: autocorrelation coefficient for the I frames of NBC News(G16B1 QP28).

ACC1	-0.11606
ACC2	0.4523
ACC16	0.86503

Table AB9b: autocorrelation coefficient for the whole NBC News trace(G16B1 QP28).

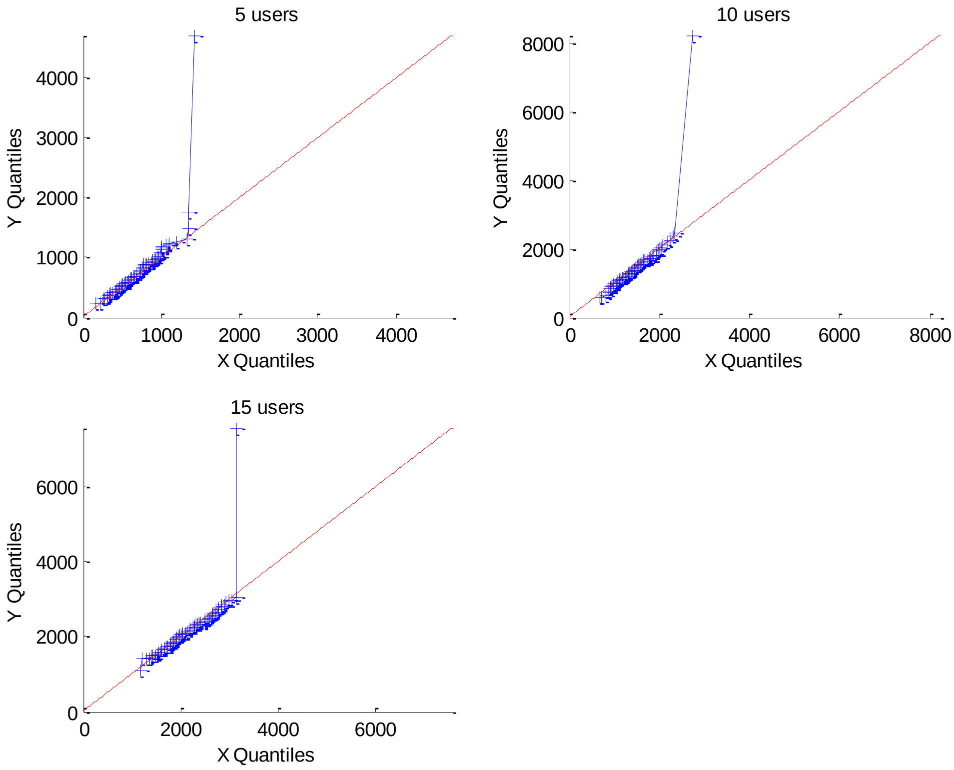

Figure AB10: Q-Q plot of the DAR(1) model versus the actual video for the P frames of NBC News(G16B3 QP38), for 5, 10 and 15 superposed sources.

ACC1	0.61761
ACC2	0.48887
ACC16	0.2637

Table AB10a: autocorrelation coefficient for the P frames of NBC News(G16B3 QP38).

ACC1	-0.064047
ACC2	-0.035215
ACC16	0.89619

Table AB10b: autocorrelation coefficient for the whole NBC News trace(G16B3 QP38).

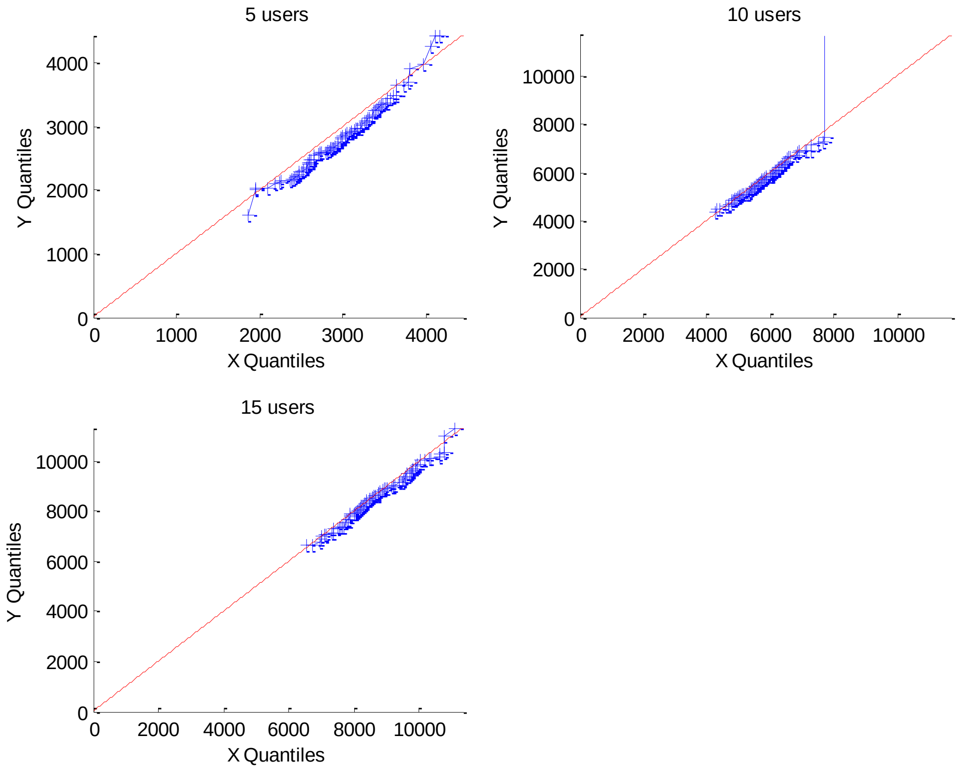

Figure AB11: Q-Q plot of the DAR(1) model versus the actual video for the I frames of NBC News(G16B7 QP38), for 5, 10 and 15 superposed sources.

ACC1	0.87394
ACC2	0.78444
ACC16	0.39897

Table AB11a: autocorrelation coefficient for the I frames of NBC News(G16B7 QP38).

ACC1	-0.031407
ACC2	0.0033238
ACC16	0.91013

Table AB11b: autocorrelation coefficient for the whole NBC News trace(G16B7 QP38).

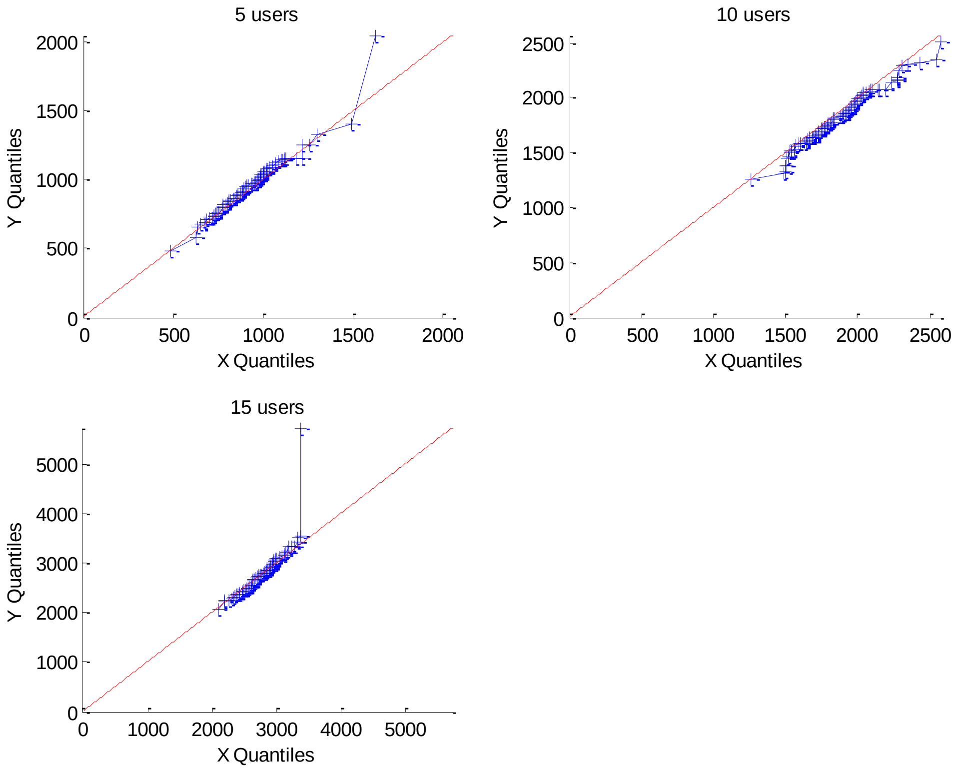

Figure AB12: Q-Q plot of the DAR(1) model versus the actual video for the I frames of NBC News(G16B15 QP48), for 5, 10 and 15 superposed sources.

ACC1	0.85556
ACC2	0.75712
ACC16	0.27305

Table AB12a: autocorrelation coefficient for the I frames of NBC News(G16B15 QP48).

ACC1	-0.028273
ACC2	-0.017128
ACC16	0.94995

Table AB12b: autocorrelation coefficient for the whole NBC News trace(G16B15 QP48).

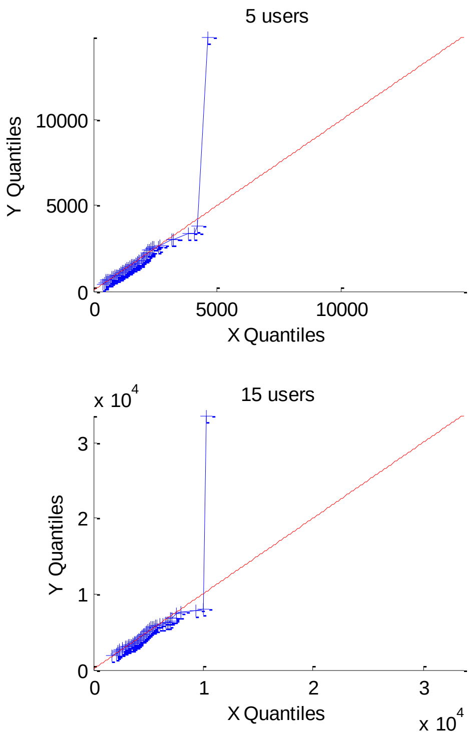

Figure AB13: Q-Q plot of the DAR(1) model versus the actual video for the P frames of Silence of the Lambs(G16B1 QP22), for 5, 10 and 15 superposed sources.

ACC1	0.88665
ACC2	0.8846
ACC16	0.81179

Table AB13a: autocorrelation coefficient for the P frames of Silence of the Lambs(G16B1 QP22).

ACC1	0.026505
ACC2	0.5185
ACC16	0.9197

Table AB13b: autocorrelation coefficient for the whole Silence of the Lambs trace(G16B1 QP22).

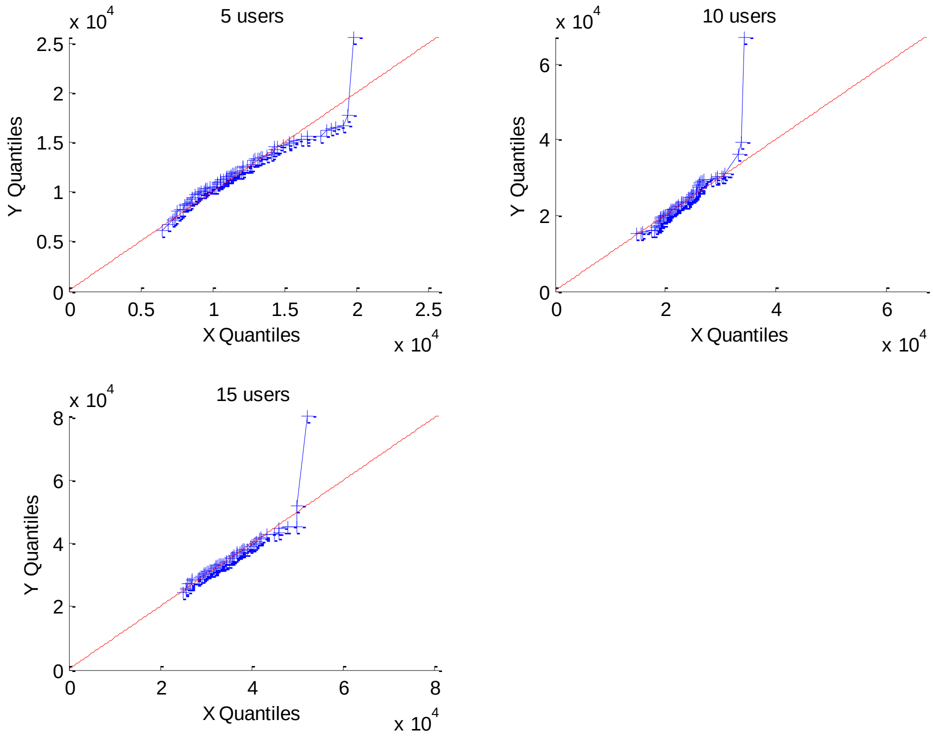

Figure AB14: Q-Q plot of the DAR(1) model versus the actual video for the P frames of Silence of the Lambs(G16B3 QP10), for 5, 10 and 15 superposed sources.

ACC1	0.87806
ACC2	0.86336
ACC16	0.71347

Table AB14a: autocorrelation coefficient for the P frames of Silence of the Lambs(G16B3 QP10).

ACC1	0.233
ACC2	0.33685
ACC16	0.87958

Table AB14b: autocorrelation coefficient for the whole Silence of the Lambs tarce(G16B3 QP10).

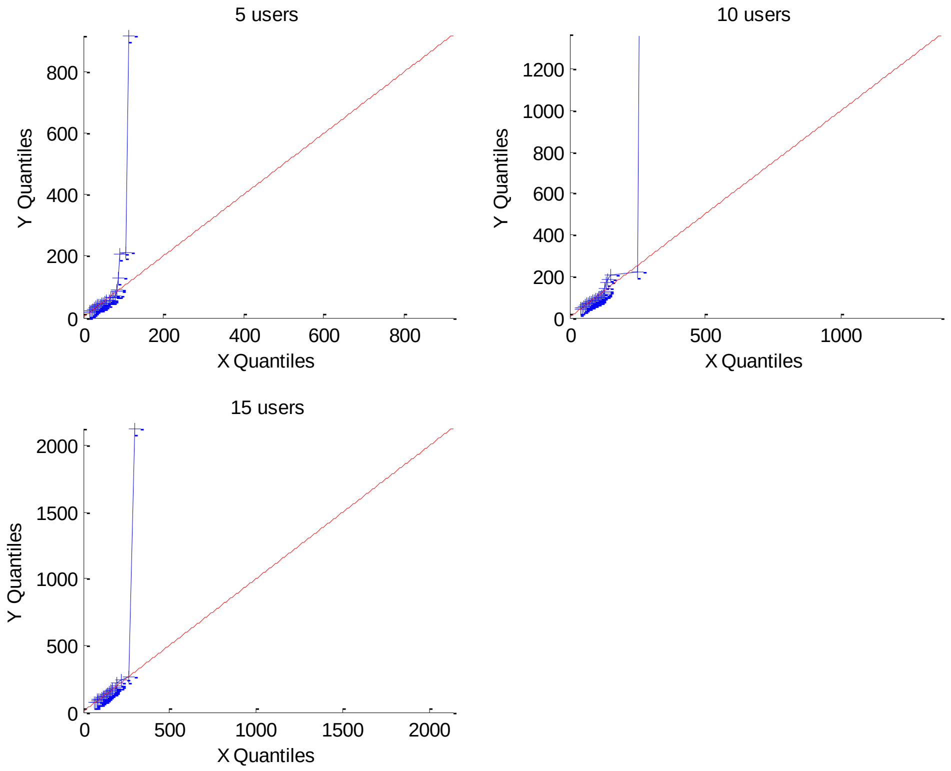

Figure AB15: Q-Q plot of the DAR(1) model versus the actual video for the B frames of Silence of the Lambs(G16B7 QP42), for 5, 10 and 15 superposed sources.

ACC1	0.91947
ACC2	0.84087
ACC16	0.73364

Table AB15a: autocorrelation coefficient for the B frames of Silence of the Lambs(G16B7 QP42).

ACC1	0.017339
ACC2	0.04086
ACC16	0.94991

Table AB15b: autocorrelation coefficient for the whole of Silence of the Lambs trace(G16B7 QP42).

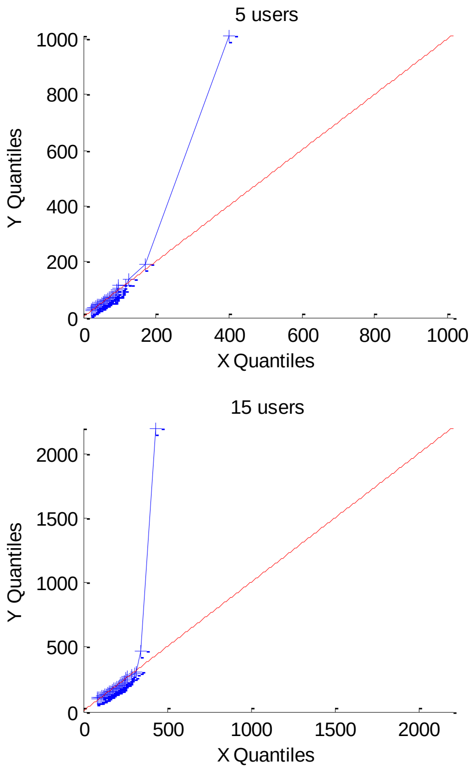

Figure AB16: Q-Q plot of the DAR(1) model versus the actual video for the B frames of Silence of the Lambs(G16B15 QP42), for 5, 10 and 15 superposed sources.

ACC1	0.95876
ACC2	0.90918
ACC16	0.82105

Table AB16a: autocorrelation coefficient for the B frames of Silence of the Lambs(G16B15 QP42).

ACC1	0.063669
ACC2	0.080241
ACC16	0.95891

Table AB16b: autocorrelation coefficient for the whole Silence of the Lambs trace(G16B15 QP42).

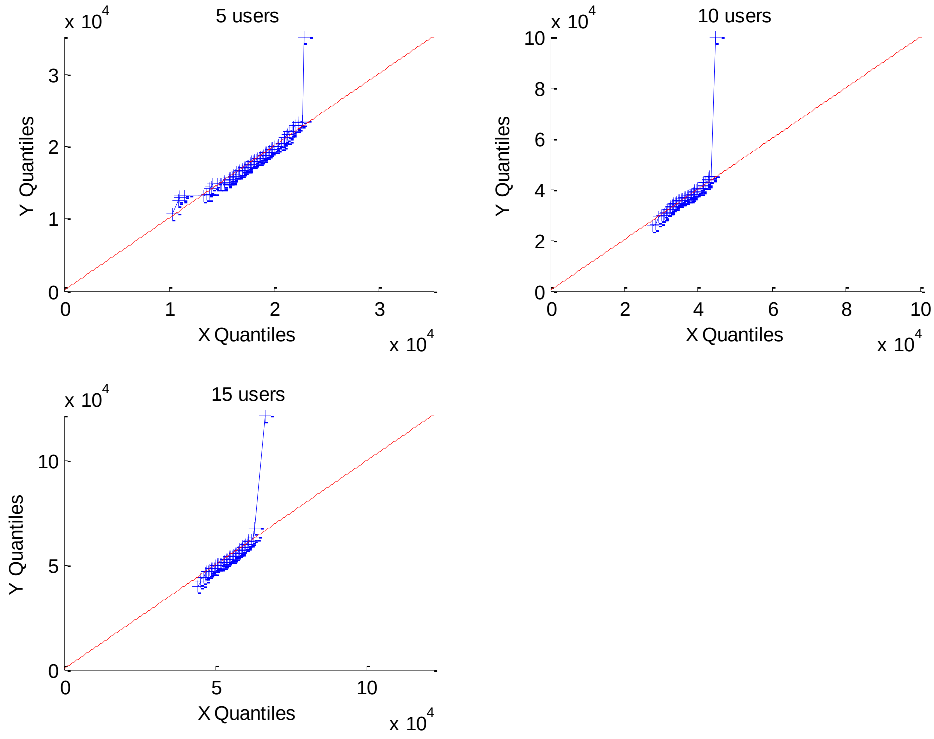

Figure AB17: Q-Q plot of the DAR(1) model versus the actual video for the P frames of Tokyo Olympics(G16B1 QP10), for 5, 10 and 15 superposed sources.

ACC1	0.89614
ACC2	0.8861
ACC16	0.77485

Table AB17a: autocorrelation coefficient for the P frames of Tokyo Olympics(G16B1 QP10).

ACC1	-0.24843
ACC2	0.57364
ACC16	0.78984

Table AB17b: autocorrelation coefficient for the whole Tokyo Olympics trace(G16B1 QP10).

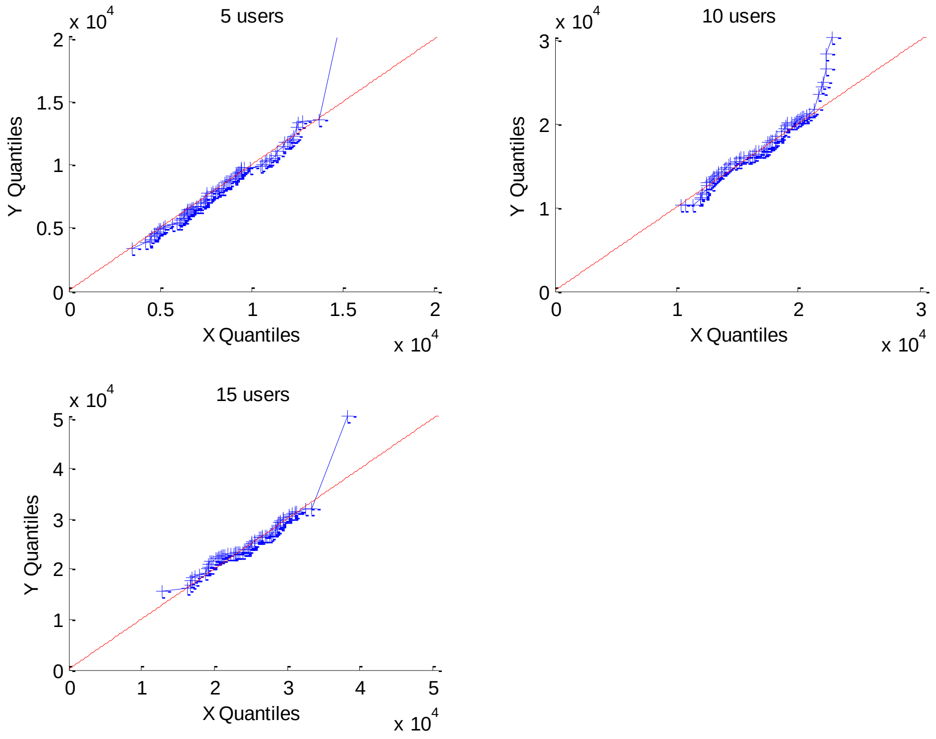

Figure AB18: Q-Q plot of the DAR(1) model versus the actual video for the I frames of Tokyo Olympics(G16B3 QP22), for 5, 10 and 15 superposed sources.

ACC1	0.94339
ACC2	0.88967
ACC16	0.48947

Table AB18a: autocorrelation coefficient for the I frames of Tokyo Olympics(G16B3 QP22).

ACC1	0.1547
ACC2	0.2475
ACC16	0.89235

Table AB18b: autocorrelation coefficient for the whole Tokyo Olympics trace(G16B3 QP22).

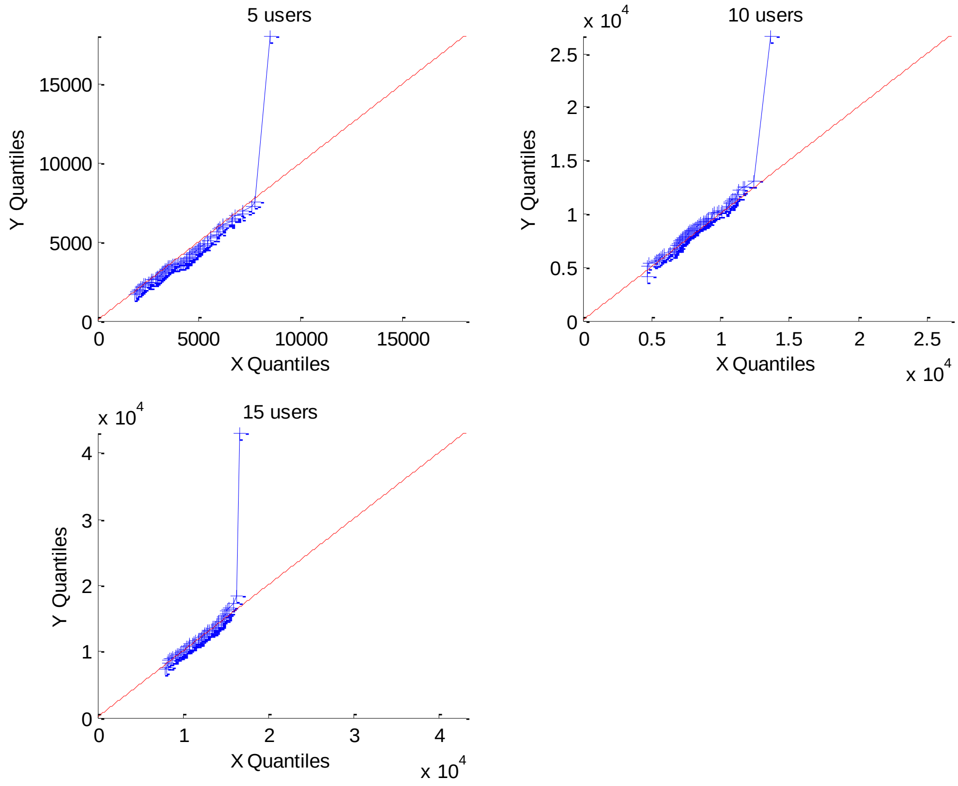

Figure AB19: Q-Q plot of the DAR(1) model versus the actual video for the P frames of Tokyo Olympics(G16B7 QP24), for 5, 10 and 15 superposed sources.

ACC1	0.85303
ACC2	0.79307
ACC16	0.43492

Table AB19a: autocorrelation coefficient for the P frames of Tokyo Olympics(G16B7 QP24).

ACC1	0.2481
ACC2	0.34086
ACC16	0.91509

Table AB19b: autocorrelation coefficient for the whole Tokyo Olympics trace(G16B7 QP24).

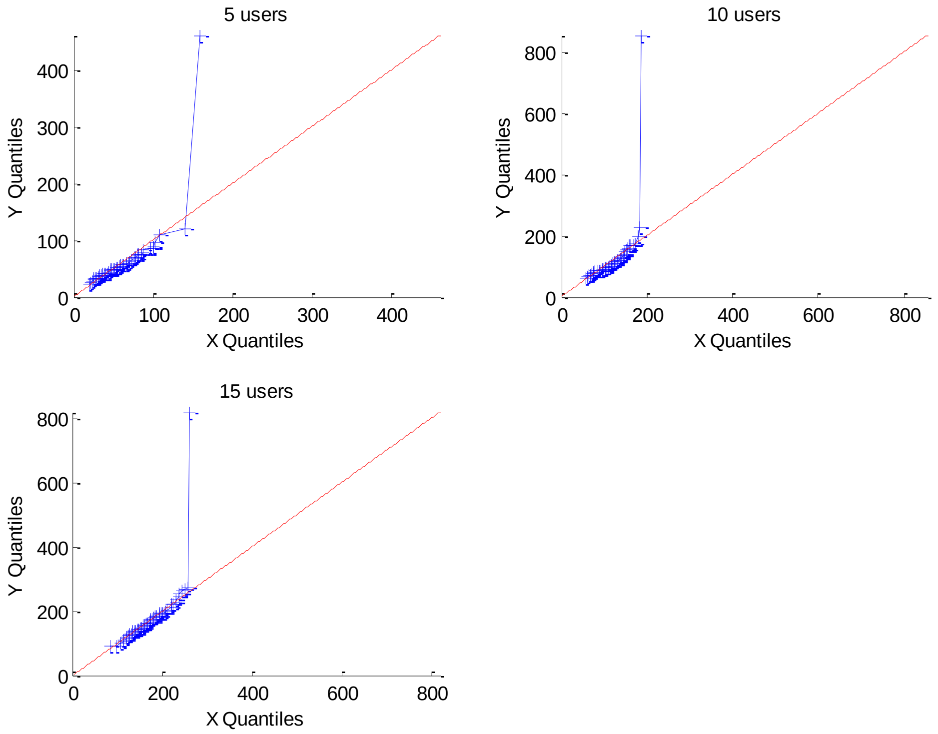

Figure AB20: Q-Q plot of the DAR(1) model versus the actual video for the B frames of Tokyo Olympics(G16B15 QP48), for 5, 10 and 15 superposed sources.

ACC1	0.95874
ACC2	0.91187
ACC16	0.76542

Table AB20a: autocorrelation coefficient for the B frames of Tokyo Olympics(G16B15 QP48).

ACC1	0.2481
ACC2	0.34086
ACC16	0.91509

Table AB20b: autocorrelation coefficient for the whole Tokyo Olympics trace(G16B15 QP48).

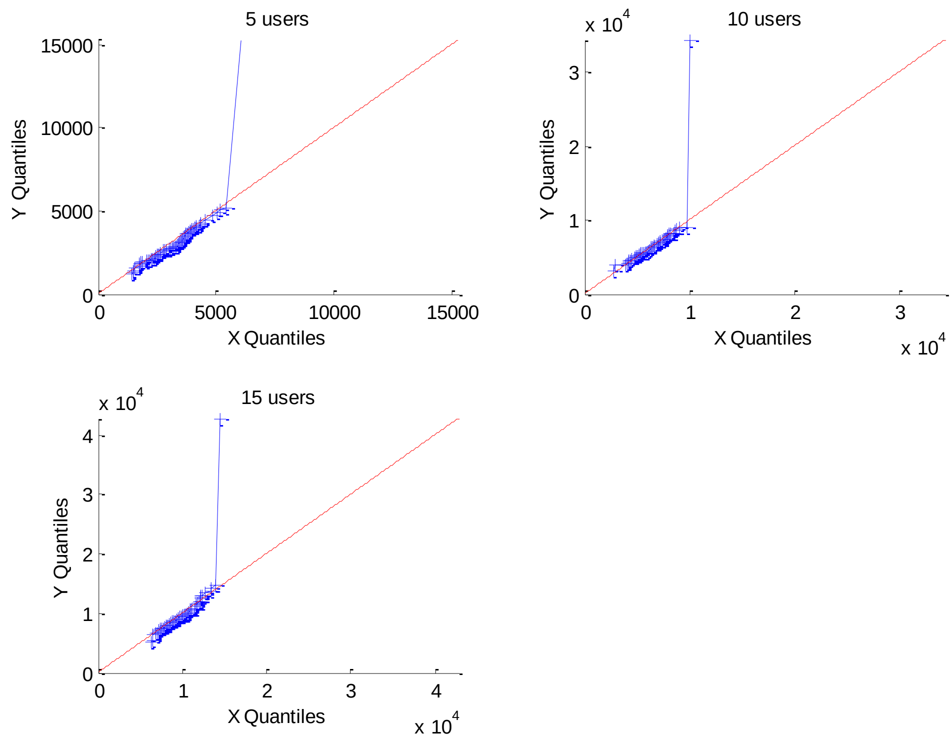

Figure AB21: Q-Q plot of the DAR(1) model versus the actual video for the P frames of Sony Demo(G16B1 QP24), for 5, 10 and 15 superposed sources.

ACC1	0.77182
ACC2	0.78788
ACC16	0.70414

Table AB21a: autocorrelation coefficient for the P frames of Sony Demo(G16B1 QP24).

ACC1	-0.20717
ACC2	0.315
ACC16	0.95689

Table AB21b: autocorrelation coefficient for whole Sony Demo trace(G16B1 QP24).

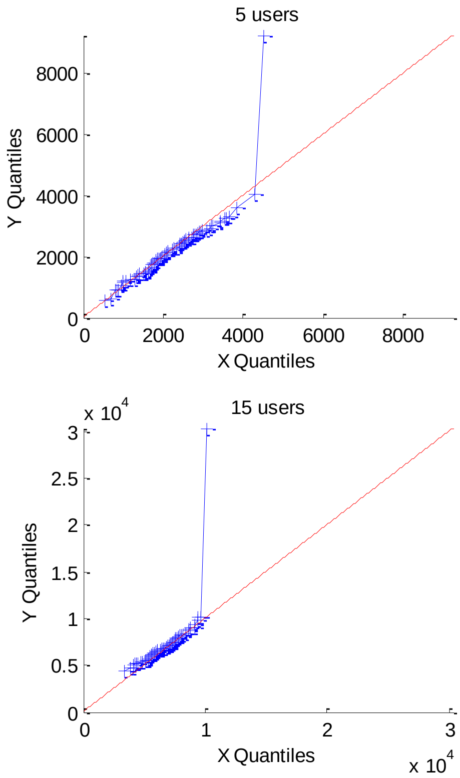

Figure AB22: Q-Q plot of the DAR(1) model versus the actual video for the P frames of Sony Demo(G16B3 QP28), for 5, 10 and 15 superposed sources.

ACC1	0.78621
ACC2	0.78146
ACC16	0.65475

Table AB22a: autocorrelation coefficient for the P frames of Sony Demo(G16B3 QP28).

ACC1	-0.092032
ACC2	-0.071513
ACC16	0.97232

Table AB22b: autocorrelation coefficient for the whole Sony Demo trace(G16B3 QP28).

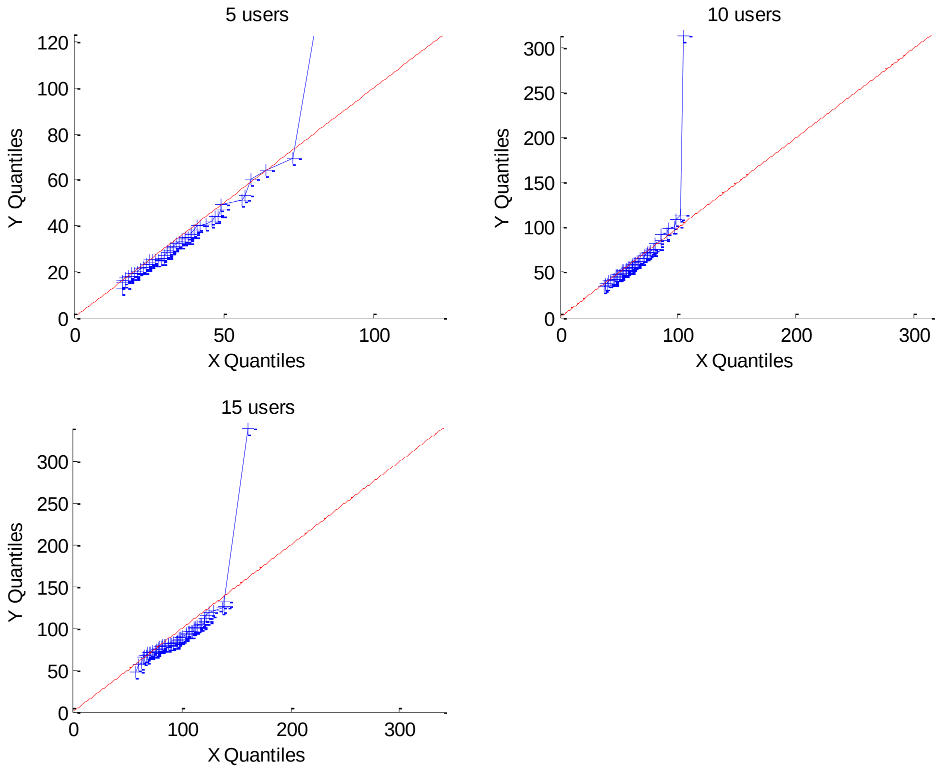

Figure AB23: Q-Q plot of the DAR(1) model versus the actual video for the B frames of Sony Demo(G16B7 QP48), for 5, 10 and 15 superposed sources.

ACC1	0.91583
ACC2	0.83746
ACC16	0.66817

Table AB23a: autocorrelation coefficient for the B frames of Sony Demo(G16B7 QP48).

ACC1	-0.062573
ACC2	-0.056392
ACC16	0.98459

Table AB23b: autocorrelation coefficient for the whole Sony Demo trace(G16B7 QP48).

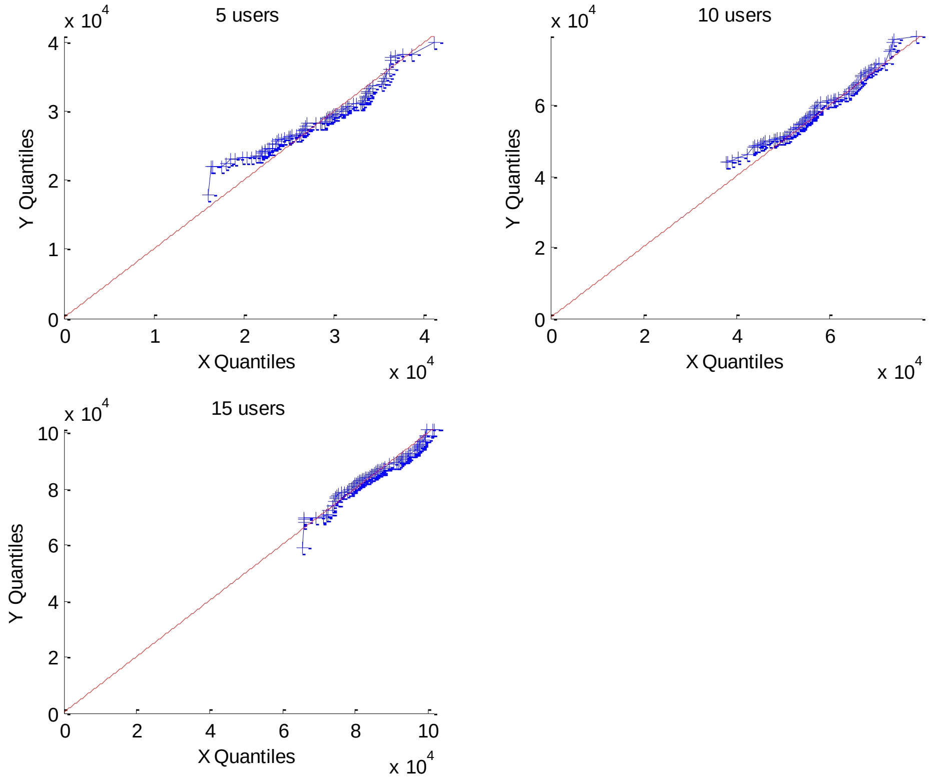

Figure AB24: Q-Q plot of the DAR(1) model versus the actual video for the I frames of Sony Demo(G16B15 QP16), for 5, 10 and 15 superposed sources.

ACC1	0.97632
ACC2	0.95395
ACC16	0.65024

Table 24a: autocorrelation coefficient for the I frames of Sony Demo(G16B15 QP16).

ACC1	0.22029
ACC2	0.28059
ACC16	0.95749

Table 24b: autocorrelation coefficient for the whole Sony Demo trace(G16B15 QP16).

Relatively accurate fitting results:

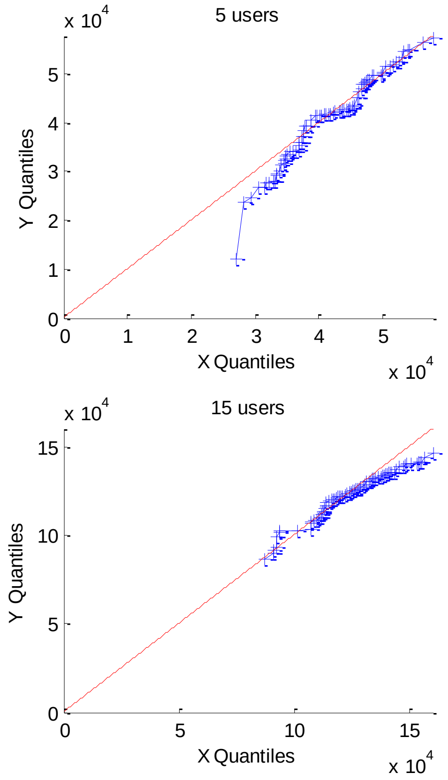

Figure AB25: Q-Q plot of the DAR(1) model versus the actual video for the I frames of Sony Demo(G16B3 QP10), for 5, 10 and 15 superposed sources.

ACC1	0.97892
ACC2	0.95754
ACC16	0.65037

Table AB25a: autocorrelation coefficient for the I frames of Sony Demo(G16B3 QP10).

ACC1	0.16837
ACC2	0.21711
ACC16	0.947

Table AB25b: autocorrelation coefficient for the whole Sony Demo trace(G16B3 QP10).

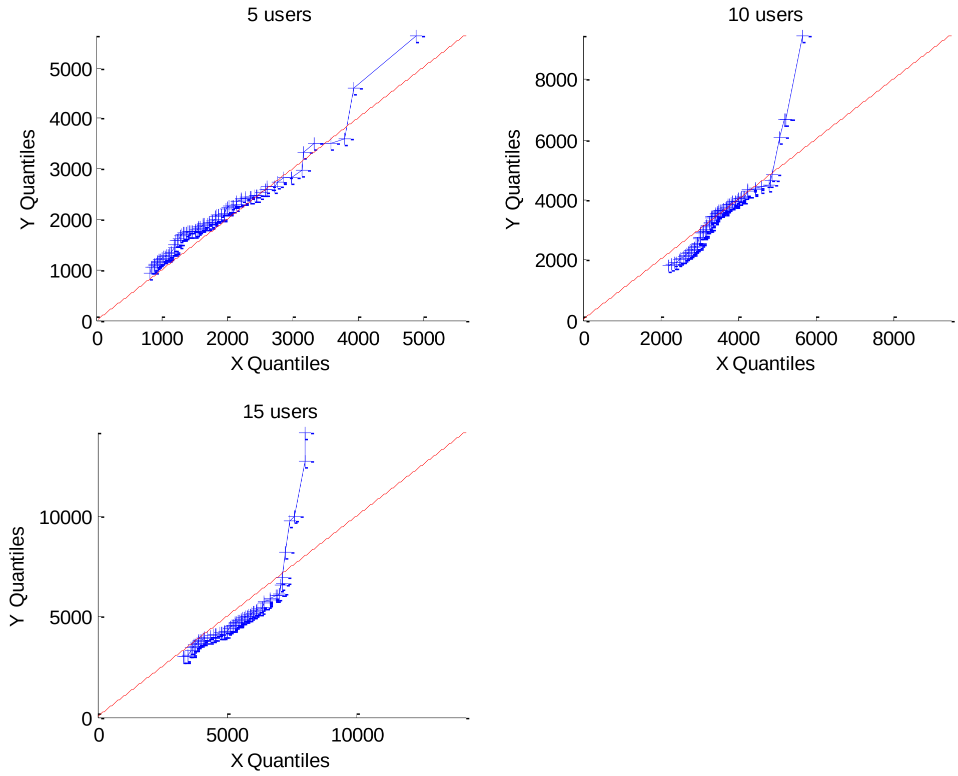

Figure AB26: Q-Q plot of the DAR(1) model versus the actual video for the I frames of Tokyo Olympics(G16B15 QP38), for 5, 10 and 15 superposed sources.

ACC1	0.99656
ACC2	0.99428
ACC16	0.96204

Table AB26a: autocorrelation coefficient for the I frames of Tokyo Olympics(G16B15 QP38).

ACC1	0.12787
ACC2	0.1673
ACC16	0.94197

Table AB26b: autocorrelation coefficient for the whole Tokyo Olympics trace(G16B15 QP38).

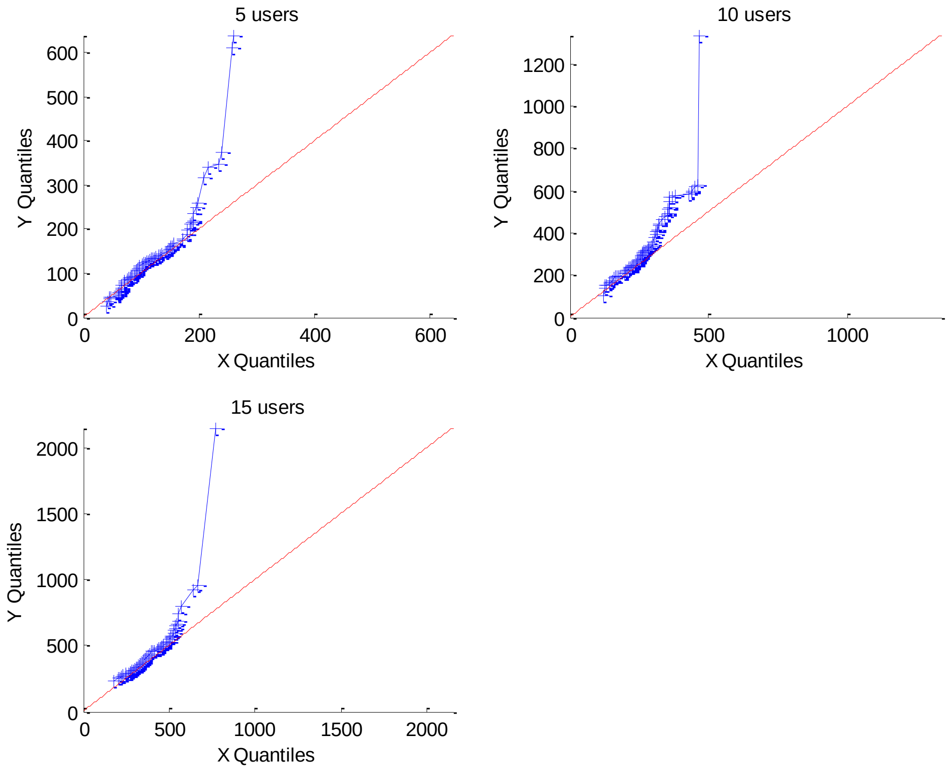

Figure AB27: Q-Q plot of the DAR(1) model versus the actual video for the P frames of Silence of the Lambs(G16B7 QP48), for 5, 10 and 15 superposed sources.

ACC1	0.70795
ACC2	0.64634
ACC16	0.3304

Table AB27a: autocorrelation coefficient for the P frames of Silence of the Lambs(G16B7 QP48).

ACC1	-0.026884
ACC2	-0.016389
ACC16	0.94433

Table AB27b: autocorrelation coefficient for the whole Silence of the Lambs trace(G16B7 QP48).

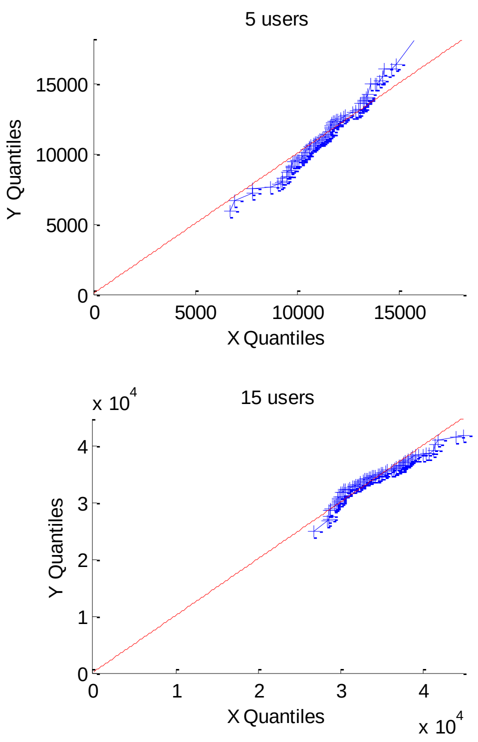

Figure AB28: Q-Q plot of the DAR(1) model versus the actual video for the I frames of NBC News(G16B7 QP24), for 5, 10 and 15 superposed sources.

ACC1	0.87759
ACC2	0.79032
ACC16	0.43691

Table AB28a: autocorrelation coefficient for the I frames of NBC News(G16B7 QP24).

ACC1	0.1649
ACC2	0.22272
ACC16	0.88008

Table AB28b: autocorrelation coefficient for the I frames of NBC News trace(G16B7 QP24).

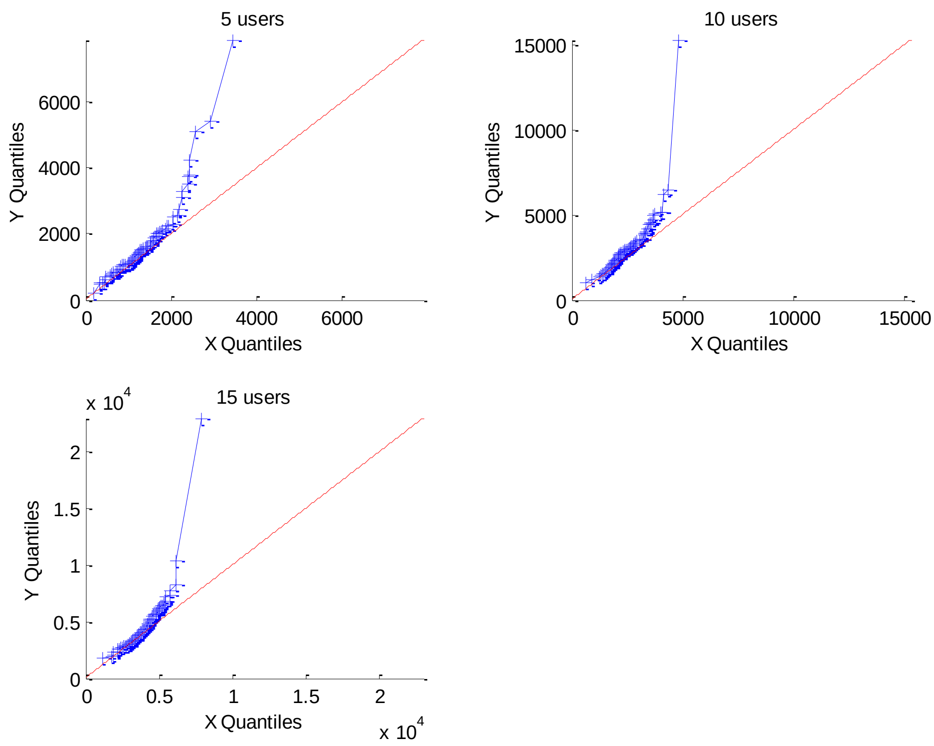

Figure AB29: Q-Q plot of the DAR(1) model versus the actual video for the B frames of Star Wars IV(G16B3 QP16), for 5, 10 and 15 superposed sources.

ACC1	0.86986
ACC2	0.83652
ACC16	0.64054

Table AB29a: autocorrelation coefficient for the B frames of Star Wars IV(G16B3 QP16).

ACC1	0.074395
ACC2	0.12102
ACC16	0.85647

Table AB29b: autocorrelation coefficient for the whole Star Wars IV trace(G16B3 QP16).

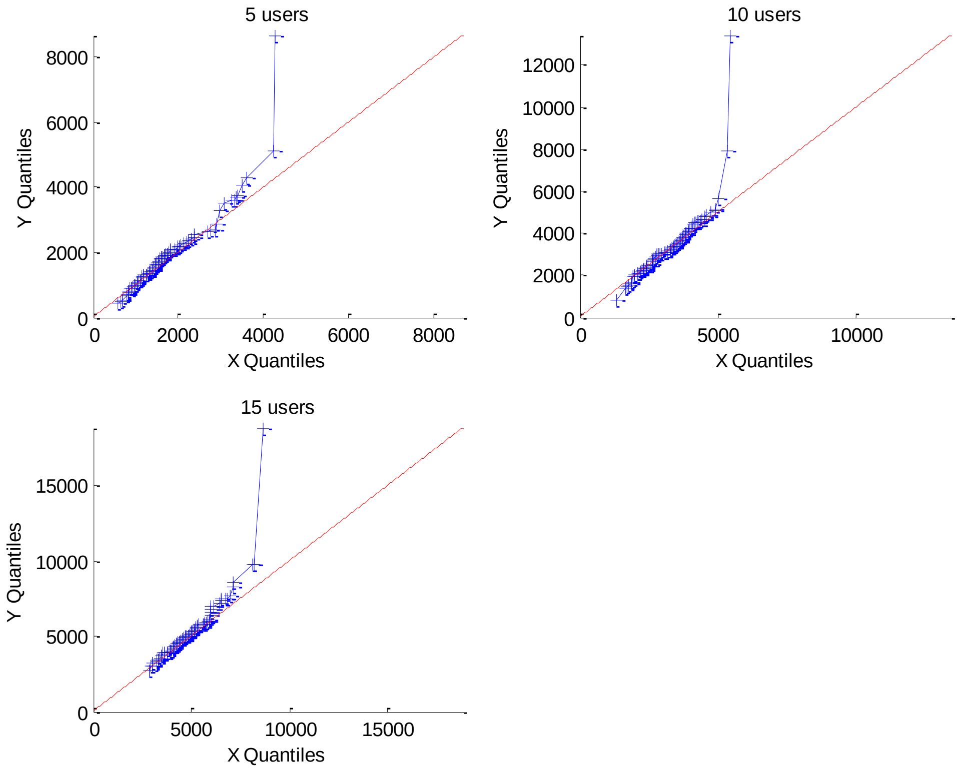

Figure AB30: Q-Q plot of the DAR(1) model versus the actual video for the B frames of Terminator(G12B2 QP34), for 5, 10 and 15 superposed sources.

ACC1	0.90881
ACC2	0.8718
ACC16	0.69609

Table AB30a: autocorrelation coefficient for the B frames of Star Wars IV(G12B2 QP34).

ACC1	-0.074752
ACC2	-0.077353
ACC12	0.9162

Table AB30b: autocorrelation coefficient for the whole Star Wars IV(G12B2 QP34).

Low accuracy results:

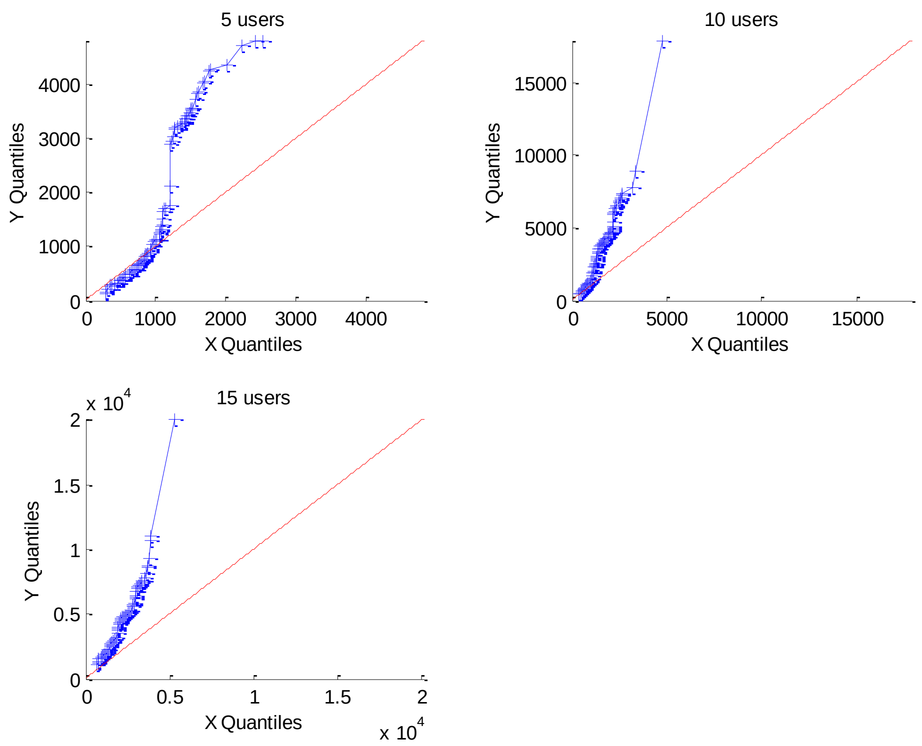

Figure AB31: Q-Q plot of the DAR(1) model versus the actual video for the B frames of Tokyo Olympics(G16B7 QP22), for 5, 10 and 15 superposed sources.

ACC1	0.059481
ACC2	0.50587
ACC16	0.021561

Table AB31a: autocorrelation coefficient for the B frames of Tokyo Olympics(G16B7 QP22).

ACC1	0.28656
ACC2	0.38276
ACC16	0.90958

Table AB31b: autocorrelation coefficient for the whole Tokyo Olympics trace(G16B7 QP22).

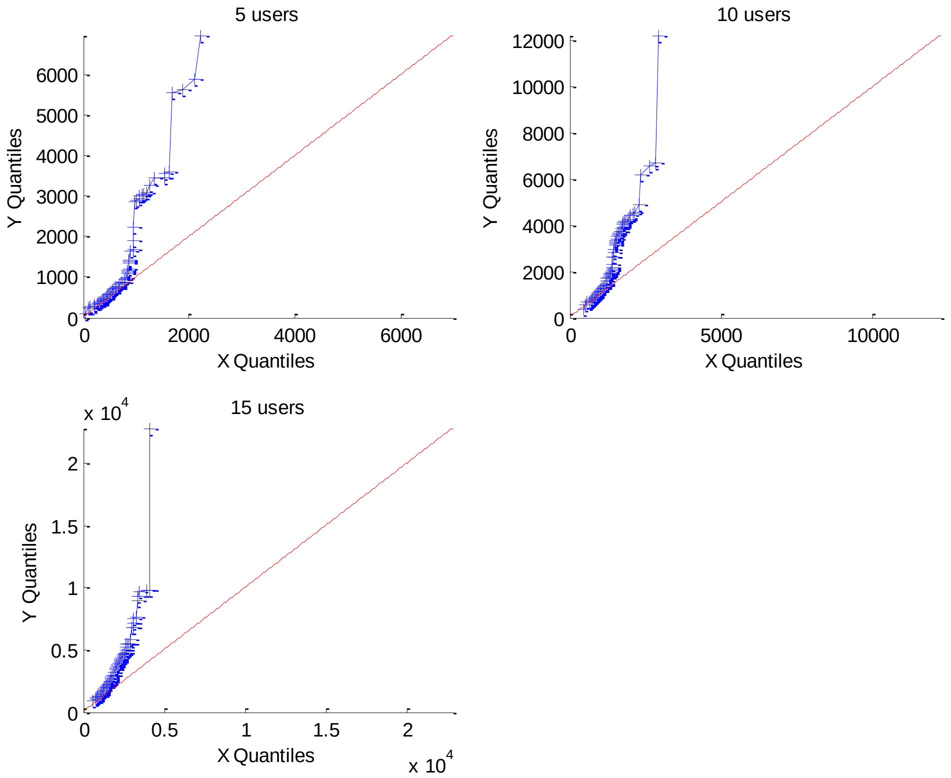

Figure AB32: Q-Q plot of the DAR(1) model versus the actual video for the B frames of Sony Demo(G16B1 QP22), for 5, 10 and 15 superposed sources.

ACC1	0.81519
ACC2	0.80366
ACC16	0.69831

Table AB32a: autocorrelation coefficient for the B frames of Sony Demo(G16B1 QP22).

ACC1	-0.21705
ACC2	0.37441
ACC16	0.95459

Table AB32b: autocorrelation coefficient for the whole Sony Demo trace(G16B1 QP22).

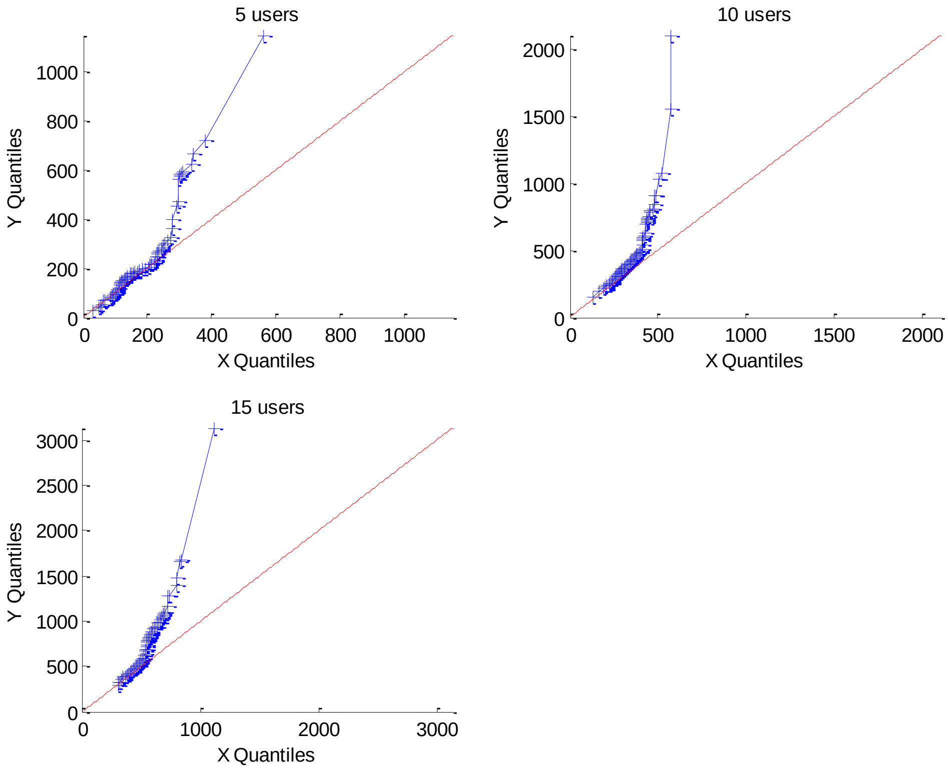

Figure AB33: Q-Q plot of the DAR(1) model versus the actual video for the P frames of Star Wars IV(G16B3 QP42), for 5, 10 and 15 superposed sources.

ACC1	0.60092
ACC2	0.54637
ACC16	0.29512

Table AB33a: autocorrelation coefficient for the P frames of Star Wars IV(G16B3 QP42).

ACC1	-0.04409
ACC2	-0.029892
ACC16	0.8974

Table AB33b: autocorrelation coefficient for the whole Star Wars IV trace(G16B3 QP42).